UNH-66-4

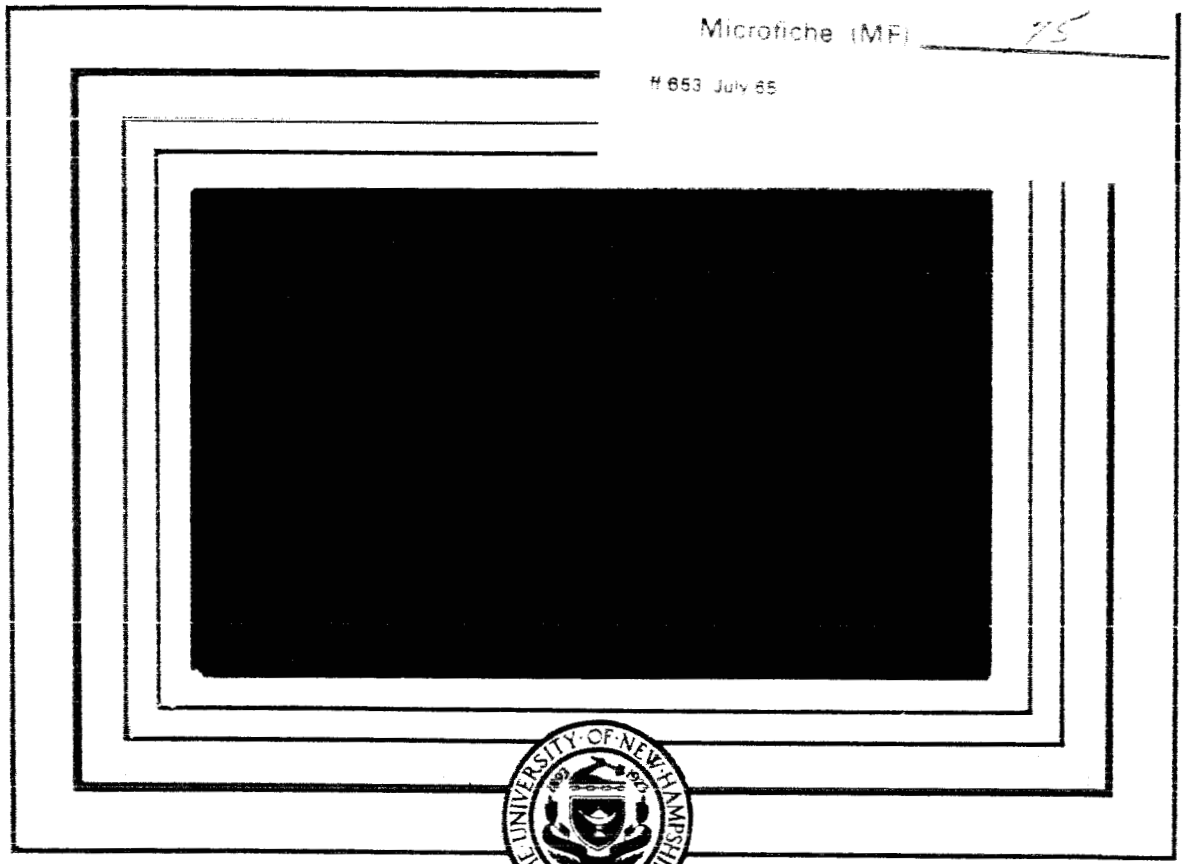

Department of Physics
UNIVERSITY OF NEW HAMPSHIRE
Durham

AN ELECTRIC FIELD METER

FOR ROCKET AND SATELLITE USE

BY

WENTWORTH EDWARDS POTTER

A THESIS

Submitted to the University of New Hampshire

In Partial Fulfillment of

The Requirements for the Degree of

Master of Science

Graduate School

Department of Physics

September, 1966

An Abstract of

AN ELECTRIC FIELD METER FOR ROCKET AND SATELLITE USE

The evidence for the existence of electric fields in the ionosphere and magnetosphere is discussed. It is seen that the charged particle motions of the atmospheric dynamo system cause electric fields in the ionosphere while plasma convections produce electric fields in the magnetosphere. The auroral and electrojet current systems are studied in relation to the electric and magnetic fields. It is proposed to make, in situ, measurements of these electric fields estimated to be 0.1 to 100 mv/m using a high impedance differential electrometer amplifier.

The ionospheric and magnetospheric media are described, and it is seen that plasma parameters have important effects on the electric field measurements. For probe measurements, the current to the probes from the plasma must be several orders of magnitude greater than the leakage current of the measuring instrument. The incident currents are found to be a function of the probe floating potential which is expected to be slightly negative in the auroral zone.

Effects such as photoemission current, sheath distortion and the induced electric field due to probe motion are studied. While the photoemission current is almost negligible, the induced field cannot be neglected and may produce errors of 100% unless it is calculated and corrections are applied to the data.

A high impedance field effect electrometer amplifier has been designed, and a description of this as well as of a rocket experiment for measuring ionospheric electric fields is presented. The system will first be used on sounding rockets and later on satellites. A unique, unfurlable probe system will be used. The accuracy of the system is expected to be $\pm$ 50% to $\pm$ 5% for measurements of 10 to 100 mv.

ACKNOWLEDGMENTS

The author wishes to express his sincere thanks to Professor Laurence J. Cahill, Jr. for his guidance and advice during the course of this research and for the numerous opportunities for advancement which he has provided. His enthusiasm has made the work more stimulating and meaningful.

The author expresses his gratitude to Mrs. Ann Bataller for her patient and excellent work in typing and assembly of the thesis and to Mr. Herbert Scheibel for the drafting work.

Special thanks go to the author's wife, Sue, for her help in typing and for her constant cheerfulness. The author is also indebted to Mrs. Phyllis Warnock for her typing assistance and to the members of the Space Science Institute of the University of California, San Diego, for their help and suggestions during the research.

The author wishes to thank the National Aeronautics and Space Administration for awarding him a pre-doctoral traineeship, which has made possible the furthering of his education.

This research was supported by National Aeronautics and Space Administration Contract NsG-624.

TABLE OF CONTENTS

LIST OF TABLES

LIST OF FIGURES

SECTION I

INTRODUCTION

Although the study of the magnetic field in space has been pursued in depth by various researchers, there has been little investigation of electric fields in space. Since these two fields are so closely related, it is now obvious that more experimentation is necessary in measuring electric fields, both in the ionosphere and in the magnetosphere.

Information gained through magnetic field experiments has led to realization of the existence of electric fields in space. Daily recorded fluctuations of the magnetic field at the earth's surface are believed to be caused by electric current systems in the ionosphere. The principal variation, with a period of one solar day, has been termed the S_q variation and it is believed to be caused by ionospheric S_q current systems. One current system that could produce the variations is in the shape of four sets of ovals, two in each hemisphere; one of these is located over the sunlit area and the other over the nighttime portion. Since the nighttime ionospheric conductivity is low, it is probable that the night system of currents is weak or absent. These current systems do not change in position relative to the sun and thus have continually changing geographical position. Daily changes in the shape of the S_q system are due to the fact that the dividing line between the hemispheric current systems is the magnetic equator which, being inclined to the geographic equator, varies in latitude between -11.5° and $+11.5^{\circ}$.

Some anomalies exist in the S_q current system, such as the auroral and equatorial electrojets which are essentially strong, localized

currents. The auroral electrojets are found near the auroral zone. Before midnight the current flow is eastward, and after midnight it is westward with a return flow across the polar cap and at lower latitudes. Another electrojet is found near the magnetic dip equator where eastward flowing current crosses the horizontal, northward-directed magnetic field. Hall polarization causes a band of enhanced conductivity known as the equatorial electrojet.

One of the most reasonable theories on the existence and cause of electric fields in the ionosphere was proposed by Stewart (1882) and has been described more recently by Chapman and Bartels (1940). The theory attributes daily geomagnetic variations to the currents above the earth. The currents are set in motion by an inductive electromotive force which is generated by the movement of the ionized gas in the presence of the geomagnetic field.

It has been suggested by Dungey (1958), Axford and Hines (1961), and others that electric fields exist in the magnetosphere as well as in the ionosphere. These theories propose convective motions of the plasma in the magnetosphere which, in the presence of the earth's magnetic field, result in the formation of electric fields in the magnetosphere. Sources of the convective motion include plasma movement due to the earth's rotation and subsequent co-rotation of the atmospheric gas and the interaction of the solar wind with the boundary of the magnetosphere.

The development of the electric field in both the ionosphere and the magnetosphere is in two parts:

1. The motion of the ionized plasma with velocity $\overline{v}$ past the $\overline{B}$ field induces an electric field $\overline{E}_i = \overline{v} \times \overline{B}$.
2. The accumulation of polarization charges causes an electrostatic field $\overline{E}_s$.

The electric field meter described in this thesis has been designed to measure, in situ, electric fields in the ionosphere and magnetosphere estimated to be 0.1 to 100 mv/meter. Since the measurements will be made from both rockets and satellites, this paper will describe not only the electric field meter but also the medium in which it will be used. The theories discussed, pertaining to the existence of electric fields and the principles of operation of the meter, indicate that the characteristics of the environmental medium are of great importance. An experiment for the measurement of electric fields from on board a sounding rocket is described in the last part of the paper.

SECTION II

THEORETICAL AND EXPERIMENTAL BACKGROUND

1. Dynamo Theory of Electric Fields

The dynamo theory, originally proposed by Stewart (1882) was later developed by Schuster (1908) who put it in quantitative form by doing a spherical harmonic analysis of the S field. The original concept has not changed greatly since then and a brief mathematical outline will be given.

Since the theory involves conductivities, it first will be necessary to quickly review the conductivities in the ionosphere. Ionospheric conductivity is greatest in the E region, 90 to 150 km, and the strongest currents can be expected there. The ionosphere is horizontally stratified so only horizontal electric fields will be effective in establishing currents. In mid-latitudes horizontal, tidal ionospheric motions perpendicular to the nearly vertical magnetic fields cause first $\overline{v} \times \overline{B}$ electric fields and then, through space charge accumulation, electrostatic fields. It is postulated also that the electrostatic field ($\overline{E}_s$) may reach higher parts of the ionosphere (since conductivity is high along $\overline{B}$) and cause currents to flow there. The plasma in these regions then moves as a result of the geomagnetic field interaction with these currents. This part of the ionosphere (F region and above) is often referred to as the "atmospheric motor".

The densities of both charged and neutral particles determine the conductivity of a gas due to their collisions. The frequency of collisions can be determined as follows (Nicolet, 1953):

The frequency of electron collisions is

$$\nu_e = \nu_{en} + \nu_{ei} \tag{1}$$

where

$$\nu_{en} = 5.4 \times 10^{-10} N_n T_e^{\frac{1}{2}} \text{ (collisions/sec)} \tag{2}$$

for electron-neutral particle collisions, and

$$\nu_{ei} = \left[34 + 8.36 \text{ Log}_{10}(T_e^{3/2}/N_e^{\frac{1}{2}}) \right] N_e T_e^{-3/2}$$

$$\text{(collisions/sec)} \tag{3}$$

for electron-ion collisions.

The ion-collision frequency has been determined by Chapman (1956) as

$$\nu_i = 2.6 \times 10^{-9} (N_n + N_i) M^{-\frac{1}{2}} \text{ (collisions/sec)} \tag{4}$$

for ion-neutral particle collisions where N_n is the neutral particle concentration (particles/cm^3), N_i is the ion concentration (ions/cm^3), N_e is the electron concentration (electrons/cm^3), T_e is the electron temperature ($^\circ$K) and M is the molecular weight of the ions and neutral particles, assuming the same mass.

The four types of conductivities found in the atmosphere are:

1. Specific (or direct) electrical conductivity (determining current flow under an electric field parallel to, or in absence of $\overline{B}$ field).

$$\sigma_o = e^2 \left[\frac{N_e}{m_e(\nu_e - i\omega)} + \frac{N_i}{m_i(\nu_i - i\omega)} \right] \tag{5}$$

where $e = 1.6 \times 10^{-20}$ emu, N_e is the electron concentration (electrons/cm^3), N_i is the ion concentration (ions/cm^3), m_e is the electron mass (gm), m_i is the ion mass (gm), and ω is

the driving frequency (collisions/sec).

2. Pederson conductivity (for current flow in the direction of an electric field which is perpendicular to the $\bar{B}$ field where one is present).

$$\sigma_1 = e^2 \left[\frac{N_e(\nu_e - i\omega)}{m_e\left[(\nu_e - i\omega)^2 + \omega_e^2\right]} + \frac{N_i(\nu_i - i\omega)}{m_i\left[(\nu_i - i\omega)^2 + \omega_i^2\right]} \right] \qquad (6)$$

where the electron cyclotron frequency $\omega_e = \frac{-B|e|}{m_e}$ and the ion cyclotron frequency is $\omega_i = \frac{+B|e|}{m_i}$. σ_1 is used to compute the electric current in the direction of the component of applied field ($\bar{E}$) that is perpendicular to the $\bar{B}$ field.

3. The Hall conductivity (for computing currents flowing perpendicular to the $\bar{E}$ and $\bar{B}$ field).

$$\sigma_2 = e^2 \left[\frac{N_e\,\omega_e}{m_e\left[(\nu_e - i\omega)^2 + \omega_e^2\right]} - \frac{N_i\,\omega_i}{m_i\left[(\nu_i - i\omega)^2 + \omega_i^2\right]} \right] \qquad (7)$$

When $\bar{E}$ and $\bar{B}$ fields are both present, both positive and negative particles drift in the $\bar{E} \times \bar{B}$ direction at the same speed (if there are no collisions); therefore there is no current. But ion collisions do occur more frequently than electron collisions, and the resulting current perpendicular to $\bar{E}$ and $\bar{B}$ is the Hall current (the Pederson current flows parallel to $\bar{E}$ and perpendicular to $\bar{B}$).

4. The Cowling conductivity, σ_3, is used in computing the energy loss per unit volume due to a current flowing in a direction perpendicular to the magnetic field. The energy loss is given by j^2/σ_3, where j is the current density (Hanson, 1961). The Cowling conductivity is

$$\sigma_3 = \sigma_1 + \frac{\sigma_2^2}{\sigma_1} \tag{8}$$

Above 170 km σ_3 is not very different from the Pederson conductivity, σ_1. It is convenient to represent the conductivities in the form of a tensor in which the direction of the magnetic field is taken along the z axis

$$\begin{pmatrix} j_x \\ j_y \\ j_z \end{pmatrix} = \begin{pmatrix} \sigma_1 & \sigma_2 & 0 \\ -\sigma_2 & \sigma_1 & 0 \\ 0 & 0 & \sigma_0 \end{pmatrix} \begin{pmatrix} E_x \\ E_y \\ E_z \end{pmatrix} \tag{9}$$

The dynamo system, previously mentioned, is located from 80 to 150 km in which electric currents exist as a result of both the $\overline{E}_s$ and $\overline{E}_i$ fields. The thin spherical shell in which the dynamo action takes place (80 to 150 km) can be treated as a shell of thickness d and uniform electrical conductivity σ. If the plasma moves with velocity, $\overline{v}$, in a magnetic field, $\overline{B}$, there will be an induced electric field in the $\overline{v} \times \overline{B}$ direction. Designating the southward, eastward, and upward components of $\overline{v}$ as v_x, v_y and v_z, respectively, and similarly with $\overline{B}$ as B_x, B_y and B_z, the components of $\overline{E}_i$ are (following Obayashi and Maeda, 1963)

$$E_x = v_y B_z - v_z B_y \tag{10}$$

$$E_y = v_z B_x - v_x B_z \tag{11}$$

$$E_z = v_x B_y - v_y B_x \tag{12}$$

Since we are considering a thin conducting shell, E_z sets up charge distributions on the surfaces of the shell which tend to cancel E_z

and thus it can be neglected. The induced electric field $\overline{E}_i$, (E_x, E_y) which is caused by a horizontal wind $\overline{v}_o$, (v_x, v_y) is seen to depend only on B_z, thus

$$E_x = v_y B_z \tag{13}$$

$$E_y = -v_x B_z \tag{14}$$

Due to the thin shell approximation, currents will only flow in horizontal directions in the shell. The current density components, j_y (eastwards) and j_x (southwards) can be derived from a current function R. In spherical coordinates (r, θ, Φ) the current density components are

$$j_x = \frac{\partial R}{r \sin \theta \partial \Phi} \tag{15}$$

$$j_y = -\frac{\partial R}{r \partial \theta} \tag{16}$$

where r is the radius of the shell.

Charge flow causes an electrostatic potential (φ) build up resulting in electric current closure thus

$$\overline{j} = \underline{\underline{\sigma}} \, (\overline{E}_i + \overline{E}_s) \tag{17}$$

where

$$(E_s)_x = -\frac{\partial \varphi}{r \partial \theta} \tag{18}$$

$$(E_s)_y = -\frac{\partial \varphi}{r \sin \theta \partial \Phi} \tag{19}$$

and $\overline{j}$ is the current density.

Using the preceding equations we find

$$\frac{\partial R}{r \sin \theta \partial \Phi} = \sigma_{xx} \left(v_y B_z - \frac{\partial \varphi}{r \partial \theta} \right) - \sigma_{xy} \left(v_x B_z + \frac{\partial \varphi}{r \sin \theta \partial \Phi} \right) \tag{20}$$

and

$$\frac{\partial R}{r\partial\theta} = \sigma_{xy}\left(v_y B_z - \frac{\partial\varphi}{r\partial\theta}\right) + \sigma_{yy}\left(v_x B_z + \frac{\partial\varphi}{r \sin\theta \partial\Phi}\right) \tag{21}$$

Eliminating φ results in the dynamo differential equation for R

$$\frac{\partial}{\partial\theta}\left(\sin\theta \frac{\partial R}{\partial\theta}\right) + \frac{\epsilon}{\sin\theta}\frac{\partial^2 R}{\partial\Phi^2} =$$

$$r\sigma_3\left[\frac{\partial}{\partial\theta}\left(v_x B_z \sin\theta\right) + \frac{\partial}{\partial\Phi}\left(v_y B_z\right)\right] \tag{22}$$

where $\epsilon = \frac{\sigma_{yy}}{\sigma_{xx}}$ which is nearly unity except at the equatorial belt where $\epsilon = \frac{\sigma_3}{\sigma_o}$. The horizontal current density for a thin layer approximation is given by

$$\begin{pmatrix} j_x \\ j_y \end{pmatrix} = \begin{pmatrix} \sigma_{xx} & \sigma_{xy} \\ -\sigma_{xy} & \sigma_{yy} \end{pmatrix} \begin{pmatrix} E_x \\ E_y \end{pmatrix} \tag{23}$$

where

$$\sigma_{xx} \approx \frac{\sigma_1}{\sin^2 I} \tag{24}$$

$$\sigma_{yy} \approx \sigma_1 \tag{25}$$

$$\sigma_{xy} \approx \frac{\sigma_2}{\sin I} \tag{26}$$

with I being the geomagnetic dip angle.

The dynamo differential equation is used to solve for the current function R. The dynamo field and the resulting charge distribution field are such as to set up a current system having some current function R. Thus when R is known the electric fields can be calculated.

Obayashi and Maeda (1963) show that an electrostatic field of 1-5 volts/km can be expected for currents on the order of 20-100 amps as

determined from geomagnetic variations of 10 - 50 γ. The principle interactions of the dynamo system are shown in Figure 1.

2. Aurora

Further evidence of the existence of electric fields in the ionosphere is found in the phenomena of auroras. The study of the auroral zones is aided by plots of isochasms (lines of equal frequency of aurora) for cloudless skys which result in ovals with centers over the auroral poles that coincide with the poles of the earth's geomagnetic axis.

The northern pole is called the boreal axis pole; in the southern hemisphere it is the austral axis pole. It is to be noted that the magnetic axis poles are different from the dip poles where B_H (horizontal) is zero. The 100% isochasms have an angular radius of approximately 23° about the pole. The line is the center of a 4° belt in which an aurora is visible on nearly every clear night. These are known as the auroral zones and they enclose the auroral caps. The frequency of displays decreases more rapidly when headed toward the equator than when headed toward the pole. The regions within 30° of each auroral pole are called the auroral regions and the 15° belts bordering these regions are the subauroral regions. The minauroral belt is located from -45° to $+45^\circ$ magnetic latitude.

The structure of the aurora is quite varied thus making it hard to describe. In periods of magnetic calm and sometimes during magnetic storms, the display may consist of faint diffuse, quiet arcs extending over part of the auroral zone. At the start of a polar magnetic storm (DP), the aurora becomes active over a wide range of longitude but esp-

ecially in the midnight sector. The active aurora and the DP storm usually are one to three hours in duration. The DP substorms may cover broad auroral strips (in latitude), and the sky shows many complicated arcs with rapid movements. Akasofu and Chapman (1962) have used both magnetograms and all-sky camera records to deduce the three-phase auroral cycle during the DP substorm.

The three phases are:

1. Quiet arcs which rise slowly from the northern horizon and move southward are followed by other arcs from the north. These arcs may or may not cross the observer's zenith.
2. The breakup period takes place as the arcs become thinner and better defined thus becoming more like waving curtains or large enclosed loops.
3. The curtains and loops disappear and leave luminous patches, up to ten minutes in duration, which often pulsate and drift eastward.

The main atomic lines of auroras, permitted and forbidden, proceed from neutral and ionized atoms of nitrogen and oxygen. The polar auroras have a distinct greenish color due to the 5577 Å forbidden line of neutral oxygen. Other forbidden lines (6300, 6364) give the red color to low-latitude auroras. Since the human eye is sensitive to the greenish light of 5577 Å, it is easily noticed. The rare type-B auroras with red borders, at least several km below normal, are due to an enhancement of the N_2 (first positive) and O_2^+ (first negative) bands. The sunlit auroras at 1000 km are violet due to fluorescence caused by the sunlight. A photo plate exposed every night for a month showed 39

lines, indicating the complexity of the auroral makeup. Such observations, however, have helped to rule out one theory as to the cause of these displays. The theory of reflected light is rejected since the light is not polarized; thus the aurora must be self-luminous.

Davis et al. (1960) and McIlwain (1960) have shown a correlation between position of high auroral luminosity and high electron flux as well as showing that the proton flux did not vary greatly over distances of approximately 40 km even though the auroral luminosity varied greatly over that distance. Further findings have indicated that both proton and electron flux are isotropic over the upper hemisphere and that a negligible particle flux was scattered back in an upward direction.

Energy fluxes of protons and electrons varied widely during the period of the experiment but were of the order of 10^{12} Kev/cm^2-sec for electrons and 10^{10} Kev/cm^2-sec for protons. The flux above 100 km was between 10^5-10^6 protons/cm^2-sec with energies near 6 Kev. In an auroral arc the energy spectrum was a nearly monoenergetic, 6 Kev electron flux of approximately 2×10^{11} electrons/cm^2-sec (McIlwain, 1960). This was reduced in quiescent displays to 10^8-10^{10} electrons/cm^2-sec. From the experimental data it appears that there is no connection between the auroras and the Van Allen radiation belt since the spectra of the electrons are greatly different.

It is expected that the aurora is caused mainly by electrons with an energy of 35 Kev or less and also sometimes by protons with energy near 100 Kev (McIlwain, 1960). According to the theory of mirror points, we find the altitude of the mirror point depends on the pitch angle θ_e of the particle when it crosses the equator. For dipole approximations, field lines have the form $r = R_e \cos^2\varphi$ so the radial

distance of the mirror point is $R_e \cos^2\varphi_m$, where φ and φ_m are the latitude and the mirror latitude, respectively. Chapman (1964) applies this to the case of auroral latitudes and finds that v_e must be small if the particle is going to mirror at 100 km. Some of the electrons mirroring at 100 km ionize the air and cause excitation of molecules to produce auroral light. As a consequence of the eastward electron drift and the westward proton drift, there is a net westward electric current resulting from the enhanced ionization with no components along the $\overline{B}$ field lines. It is to be noted that the total fluxes may be unequal because the latitude band covered by the precipitated protons is greater than that for the electrons. This is shown by the distribution of the hydrogen light in the aurora.

The existence of the varying electric currents due to auroras implies the existence of electric fields. Thus, by measuring the electric field at heights between 100 km and 150 km, we should be able to gain further information on the cause and structure of auroral displays. Near magnetic midnight there appears to be a reversal of the electric current accompanied by a change in both auroral form and activity. This change along with the change in direction of auroral motion implies there will be a reversal of the electric field near magnetic midnight. This change might be detected by flying rockets through this zone.

Above 150 km the conductivity along the $\overline{B}$ field lines is much larger than the other conductivities so that the $\overline{B}$ field lines become lines of equal electric potential. Thus a nearly one-to-one mapping of the ionospheric potentials into the magnetosphere should be obtained (Axford and Hines, 1961). For most model atmospheres $\sigma_2 \gg \sigma_1$, and the

electric field is expected to be close to perpendicular to the current system. Since the current flow at auroral latitudes is in the east-west direction, we normally expect $\bar{E}$ fields horizontal to the earth's surface but in a north-south direction. Due to the many arcs and other forms of aurora, it is expected, however, that occasionally $\sigma_1 \gg \sigma_2$, in which case the horizontal $\bar{E}$ field would be in an east-west orientation. Layers of arcs or rayed forms might reasonably show horizontal $\bar{E}$ fields in many directions when electric field measurements are made as a vehicle passes through them. Knowledge of this type is expected to be quite helpful in understanding the aurora and current systems.

3. Electric Fields in the Magnetosphere

It has been suggested by Dungey (1958), Axford and Hines (1961), and others that electric fields exist in the magnetosphere (Gold, 1959) as well as in the ionosphere. The boundary of the magnetosphere has usually been defined as a surface where the plasma kinetic energy and the magnetic energy density are equal.

$$\frac{B^2}{8\pi} = 2\, mnv^2 \cos^2\psi \tag{27}$$

where ψ is the angle between the normal to the boundary surface and the initial direction, v is the initial velocity of the plasma protons, m is the mass and n is the number density.

The general shape of the boundary (magnetosphere) is hemispherical on the earth's sunlit side, while in the anti-solar direction, it is believed to extend back into a tail. The solar-side boundary is believed to be near 10 R_e (Cahill and Amazeen, 1963), (Ness, 1964), while the tail

may extend out farther than 70 R_e (Cahill, 1965). The streaming protons and electrons (solar wind) ejected from the sun tend to shape the magnetosphere into its "tear-drop" shape in which the geomagnetic field is confined and compressed. Thus, in general, the magnetosphere may be defined as a region between the earth's lower atmosphere and interplanetary space where the earth's magnetic field affects the particle motion.

There exists a co-rotation of the atmospheric gas with the earth which also implies a movement of the magnetospheric field and plasma if one considers the frozen field concept as valid (Alfvén, 1963). Plasma motion across field lines would lead to an induction field $\overline{E}_i = \overline{v}_r \times \overline{B}$ ($\overline{v}_r$ is the rotational velocity vector). For a steady state (co-rotation) to exist, $\overline{E}_s + \overline{E}_i = 0$, where $\overline{E}_s$ is a polarization field which must be set up to offset the Lorentz force.

It is felt by many that convective motion exists throughout the outer magnetosphere. Axford and Hines (1961) have shown that convective motion could exist in the tail region due to the viscous interaction between the plasma and the solar stream. By setting up a polarization field directed westward, it is seen that inward convection from the tail can proceed into the magnetosphere. They assume that high latitude magnetic field lines form closed loops which are confined by the tail of the magnetosphere. They further suggest that at the border between the inner, co-rotating magnetosphere and the tail there exist "zones of confusion" where the magnetic field shows many irregularities.

To show that convection of plasma in the magnetosphere exists, it must further be assumed that some of the solar wind momentum is transferred across the boundary of the magnetosphere. As the solar wind passes around the earth, it carries material in the outer regions

of the magnetosphere away from the sun to the tail. It will stay in the magnetosphere since it is linked to the geomagnetic field. The return flow of the ionized particles, therefore, must be at the center of the tail, proceeding back toward the dark side of the earth. Since the ionization is "frozen" to the field lines, they will carry out the convective motion.

One naturally expects the existence of electric fields since, due to convective motion, there is an ionized medium crossing $\overline{B}$ field lines with a velocity $\overline{v}$. To offset the Lorentz force we can assume the existence of a polarization field which is derivable from a potential ϕ where

$$\overline{\text{grad}}\ \phi = -\overline{E} = \overline{v} \times \overline{B} \tag{28}$$

where $\overline{v}$ lies in the equipotential surface which includes the local $\overline{B}$ vector. The theory of Axford and Hines (1961) further states that the magnetic field lines are equipotential, thereby implying that the existing electric fields must be mapped along the field lines to other regions of the magnetosphere.

Dungey (1961) proposed a theory in which the tail might be open. If the interplanetary magnetic field is parallel but opposite to the earth's field at a neutral point in the sunlit hemisphere, it might join the earth's magnetic field. With the magnetosphere plasma anchored to them after connection, the outer field lines would be drawn toward the tail by the solar wind which was perpendicular to the interplanetary field lines at the nose. At the rear of the magnetosphere, the interplanetary field lines are detached from the earth's field. The plasma in the tail region returns in a convective motion (similar to the

Axford and Hines convection) to the front of the magnetosphere with field lines that enter the auroral zone.

The model proposed by Dungey also explains the electric current produced by the $\bar{v} \times \bar{B}$ fields previously discussed. The currents of this model, as before, flow east to west along the auroral zone in the dawn hemisphere. In the dusk hemisphere they flow west to east and, as before, they have a closed loop flow back across the polar cap. Dungey believes that these currents extend down to the ionospheric level thus providing a source of the auroral electrojet.

4. Previous Experiments Concerning Electric Fields

The interest in the electric fields of the atmosphere and of space is by no means new. Experimenters such as Currie and Kreielsheimer (1960), Mapleson and Whitlock (1955), and Paltridge (1964), have made numerous measurements of the earth's electric field on the earth's surface and in the lower atmosphere. The basic apparatus used in these measurements is the mechanically driven "field mill". Essentially, it consists of a rotor which is alternately exposed to the atmosphere and to a grounded stator. When the rotor is exposed to the field, a proportional charge is induced on it. The rotor moves to a screened position where it is connected to an electrometer for the measurement of the charge. It is then grounded and again exposed to the field thus providing a continuous measurement of the electric field. When the rotor is cycled fast enough, the electrometer receives a sequence of current pulses and acquires a steady potential proportional to the field being measured.

Various refinements of this procedure have been made, such as employing a double-ended mill with two rotors and using a variety of rotor shapes and materials. Another method employed by Paltridge (1964)

was to support conducting discs at different distances below a balloon. The charge induced on this "capacitor" type of arrangement was then measured by an electrometer.

These methods have proven satisfactory at altitudes up to 30 km, where the field is in the range of 1 v/m at 30 km up to 250 v/m on the earth's surface. It has been noted, however, that at rocket and satellite altitudes one expects a much smaller electric field on the order of millivolts. Imyanitov and Shvarts (1963) and Bourdeau et al. (1961) used field mills in satellite applications (Sputnik III and Explorer VIII) without meaningful results since they lacked the sensitivity required. Whipple (1965) suggests that the ultimate sensitivity possible with field mills will probably be on the order of 1 v/m which is much larger than the expected fields in space. Another factor to be considered is that the field mills are quite sensitive to direct currents flowing to the vehicle from the plasma which is undesirable as is the fact that the field mill would respond first to the sheath field which always surrounds the space craft. Thus the use of field mills in high altitude work appears to be unfeasible.

Another method of electric field measurement has been tried by Kavadas (1965) in which the ejectable probes eliminate the problems of the sheath surrounding the mother vehicle. Each ejected package contained an electrometer and transmitter and consisted of two sections separated by insulation. Measurements were also made on board the rocket using an A.C. differential amplifier with flushmounted probes aligned parallel and perpendicular to the axis of the rocket. Since the rocket spin rate was known, the sinusoidal variation of the resultant signal was expected. The ejected packages were tumbling and thus also gave a sinusoidal signal with the electric field variation superimposed.

Since the probes on the rocket were flush, there were effects due to the plasma sheath as well as the "pile up" effect of slower moving ions. The tumbling packages presented some ambiguity in the field direction and concerning the data as a whole. Kavadas states, "The interpretation of the measurements proved extremely complex and a number of ambiguities could not be completely resolved". In general, however, the range of $\bar{E}$ fields was on the order of 20-100 mv/m.

From these past attempts it appears that a more feasible method of $\bar{E}$ field measurement is to extend probes on booms away from the vehicle body and to determine the potential difference between them by measuring the small current drawn between them ($\sim \pm 10^{-11}$ amps) with high impedance electrometer perhaps as high as 10^{11} Ω. As of now, there have been no measurements using this technique; however, Aggson and Heppner (1964, 1965) have proposed that this type of experiment should be flown on A.T.S. #1 and POGO series of satellites. The technique that they propose is similar to the one discussed in this paper.

There are many benefits to be gained from the measurement of the electric field in space. As mentioned earlier, it is felt that there is a close association between the aurora and the electric fields. Measurements conducted in the magnetosphere may provide a valuable insight into the current system and the magnetic field there. Not only is there interest in the electric fields themselves, but in the correlation between them and other parameters in the magnetosphere, such as magnetic field fluctuations, plasma waves, electrojets and magnetic, field-aligned irregularities.

The rocket flights of the electric field meter described in this paper are planned for early in 1967 and should be among the first such tests of this technique. It is apparent that if one hopes to develop

more sophisticated theories of the magnetosphere, there will have to be much more data acquired concerning the electric field in space. It is felt by the author that this technique will provide worthwhile data on these electric fields as well as leading to further refinements in the technique of electric field measurements in space.

SECTION III

THEORY AND DESIGN OF ELECTRIC FIELD METER

1. Description of Environmental Medium

a. The Ionosphere. To understand the theory of the electric field meter, it is necessary to describe briefly the medium in which it will be used. In describing the upper atmosphere, a model atmosphere similar to that discussed by Sagalyn (1963) will be used. In this, the ionosphere is divided into several regions, namely the D, E, F_1, and F_2.

For all practical purposes the lower and upper limits of the D region are at 60 km and 100 km, respectively. The ionization and recombination processes in the region are not yet well understood. Some of the important sources of ionization are the photoionization of NO by Hydrogen Lyman α at 1215 $\mathring{A}$, which results in the production of ions and electrons and the ionization in this region due to cosmic radiation. Below 90 km ionization occurs due to X-rays (1-30 $\mathring{A}$), while between 90-100 km it is due partially to the flux of solar ultraviolet (below 1000 $\mathring{A}$).

Electrons are mainly produced by collisional detachment and photodetachment from negative ions. The most significant recombination process for positive ions is called dissociative recombination. Negative ions are lost in the photodetachment process. Since photodetachment and photoionization play a role in determining the atmospheric composition, one can explain the diurnal variations found by experiments. During the night the D region nearly disappears since the electron concentrations

become very low. The maximum electron concentration occurs near 80 km ($\sim 10^3$ electrons/cm^3).

In the E region (100-160 km) both the temperature and mean free path increase with altitude. During the day X-rays (10-170 Å) and solar ultraviolet (170-1026 Å) produce electrons and ions. The composition changes quite rapidly after sunset, and the ionization drops due to the high ion concentration and the dissociative recombination.

Sporadic E ionization, not yet fully understood, consists of irregular, sharp rises in ionization found in the lower E region. In lower regions of the ionosphere the electron and ion densities are similar (except for the negative ions found in D), since they are formed and eliminated in pairs. There is also a variation in electron concentration that occurs simultaneously with the sunspot cycle. During sunspot minimum the electron concentration is $\sim 10^5$ electrons/cm^3 (at noon); this may rise 50% during sunspot maximum.

The boundaries between the regions are not exact by any means, but it is generally accepted that the F_1 region has limits of 160-220 km. Electron production is due to photoionization (solar ultraviolet 200-1000 Å, and He II 304 Å line of the solar spectrum). It is interesting to note that the electrons during the day, due to their initial high energy (i.e. velocity), have much higher temperatures than do the ions. The composition varies from NO^+ to O_2^+ at lower altitudes to O^+ at higher altitudes. The electron concentration again varies with the sunspot cycle, being $\sim 2.5 \times 10^5$ electrons/cm^3 during sunspot maximum (at noon). During the night the electron concentration drops below 10^4 electrons/cm^3 and is not easily detected.

Ion-atom exchange processes account for the loss in oxygen ions at night, while electrons are lost by dissociative recombination with NO^+

and O_2^+.

The F_2 region has no set outer boundary, but it can be arbitrarily put at 1300 km. In general, the recombination rate falls off more rapidly with altitude than does the ionization rate resulting in higher ion concentration at higher altitudes. O^+ is the predominant ion. The electron concentration varies greatly with such factors as sunspot cycle, latitude and time of day. The maximum concentration is usually found between 200 - 400 km.

At 1300 km protons are found to be the primary ions present. They are formed by charge exchange between neutral hydrogen atoms and atomic oxygen ions. Photoionization creates a negligible contribution. The maximum proton concentration is near 1300 km and is $\sim 5 \times 10^3$ protons/cm^3. Since photoionization is minimal, there are only minor diurnal variations in particle density here. Above 1300 km the ion concentration falls off very slowly with altitude. Much of the information on electron densities at high altitudes has been gained through the study of "whistlers" which propagate in this medium. Whistlers are bursts of very low frequency electromagnetic energy produced by lightning which travel along the $\overline{B}$ field lines between mirror points. Their dispersion is a function of both path length and electron density.

b. Particle Motion in Plasmas and Plasma Properties. To realize the problems one might encounter in the measurement of the electric field, it is necessary to review the characteristics of charged particle motion in a plasma under the influence of $\overline{E}$ and $\overline{B}$ fields. As is customary, it is most convenient to first consider only static uniform $\overline{E}$ and $\overline{B}$ fields. Since the probes will only be a few meters apart, no appreciable spatial irregularities are expected in the $\overline{E}$ and $\overline{B}$ fields. Since the principal forces acting on the particle will be electric and magnetic, the equation

of motion (neglecting gravity) is written as Newton's second law.

$$\bar{F} = m \frac{d\bar{v}}{dt} = q\bar{E} + q\bar{v} \times \bar{B} \tag{29}$$

where $\bar{v}$ is the instantaneous particle velocity, q is the particle charge and $\bar{E}$ and $\bar{B}$ are the electric and magnetic fields, respectively.

When the external applied $\bar{E}$ field is zero the Lorentz force on the particle charge q is

$$\bar{F} = q\bar{v} \times \bar{B} = qvB \sin \theta \tag{30}$$

where θ is the angle between $\bar{v}$ and $\bar{B}$. For a positive charge $\bar{v}$, $\bar{B}$ and $\bar{F}$ are given by the right hand rule (respectively, thumb, index and middle fingers). For a negative charge (-q) the force will be in the opposite direction. Noticing the properties of the cross product, it is seen that if the particle velocity $\bar{v}$ is in the direction of $\bar{B}$, the sin θ = 0 and therefore $\bar{F}$ = 0. For other values of θ a force exists.

We can look at the force when $\theta = 90^{\circ}$ and +q is moving perpendicular to the $\bar{B}$ field. No work is done and the force can't alter the magnitude of the velocity. At equilibrium, the particle moves in a circle about $\bar{B}$ with the centripetal force provided by the Lorentz force on q, thus

$$\frac{mv^2}{R} = qv_{\perp} B \tag{31}$$

where m is the mass of charge q.

Solving for R,

$$R = \frac{mv_{\perp}}{qB} = \frac{mv}{qB} \sin \theta \tag{32}$$

where R is known as the cyclotron radius. Thus, for initial particle motion perpendicular to $\bar{B}$ field lines, the particle will move in a

circular path about the field line. If θ is not 90°, the velocity will have two components relative to the $\overline{B}$ field lines. From the previous discussion it is to be expected that the $\overline{B}$ field will not have any effect on the component parallel to itself and will affect only the perpendicular velocity component ($v_{\perp}$). Since the $v_{\perp}$ component results in a circular particle motion about the field line, the $v_{\parallel}$ component (parallel to $\overline{B}$) will lead to a helical combination of rotational and translational motion.

For the motion of a charged particle (+q) in a uniform electric field ($\overline{E}$) we can look at the definition of the electric field $\overline{E} = \frac{\overline{F}}{q}$. The force on q is along $\overline{E}$ and the particle motion is determined as in the following example, as seen in Figure 3. If a positive particle has an initial velocity in the y direction, v_y and it enters a perpendicular E_z field, the particle is deflected down with acceleration $a_z = \frac{qE_z}{m}$. From the displacement equation $z = \frac{1}{2} at^2$, we find the z displacement to be

$$z = \frac{qE_y^2}{2mv_y^2} \tag{33}$$

which is a parabolic trajectory.

In the magnetosphere and ionosphere $\overline{E}$ and $\overline{B}$ are found at various orientations to each other. Still assuming uniform fields, we can study particle motion when $\overline{E}$ is parallel to $\overline{B}$, perpendicular to $\overline{B}$, and at some angle θ with respect to $\overline{B}$.

When $\overline{E}$ is parallel to $\overline{B}$, it will accelerate or decelerate the particle independently of the $\overline{B}$ field since the motion will be along $\overline{B}$. At the same time, however, the $\overline{E}$ field will not affect the particle motion in the plane perpendicular to $\overline{B}$. The resulting motion will then be a helix, the radius of which is either expanding or contracting,

depending on the directions of $\bar{E}$ and $\bar{B}$ as well as the particle charge sign (Figure 4). If the particle does not initially have a v_z or v_x component velocity, it will move along the y-axis with a constant acceleration.

Another case is when $\bar{E}$ is perpendicular to $\bar{B}$. For the field diagram in Figure 4, a particle with positive charge and zero initial velocity is accelerated in the direction of the z-axis. Since the force due to $\bar{B}$ increases with increasing velocity ($v_\perp$), perpendicular to $\bar{B}$, it will tend to drive the particle back to the y-axis. As the particle curves back, the $\bar{E}$ field tends to retard the motion, and its velocity will approach zero, whereupon it will repeat the cycle. The time for one cycle is the cyclotron period and is equal to

$$\tau = \frac{2\pi m}{qB} \tag{34}$$

It is to be noted that the electron has the same direction of motion as the positive ion although the loops are smaller due to its smaller mass. All components of the plasma drift with equal velocities

$$\bar{U}_d = \frac{\bar{E} \times \bar{B}}{B^2} \tag{35}$$

since $\bar{U}_d$ does not depend on the charge, mass or velocity of the particle.

When $\bar{B}$ is not variable with time but non-uniform in space, the following analysis can be used. If the particle has a small Larmor radius, it will make many revolutions before it passes through a region of considerable change in $\bar{B}$. If $|B|$ is increasing there is a transverse component of $\bar{B}$ as well as the component along the axis of the helix. The resultant $\bar{v} \times \bar{B}_{trans}$ force retards the motion of the particle towards increasing $\bar{B}$. The pitch angle between $\bar{v}$ and $\bar{B}$ increases and the particle

velocity along the field lines decreases to zero at the "mirror points". It is noted that the total velocity of q in a $\overline{B}$ field is constant; therefore, the deceleration of motion along $\overline{B}$ toward the stronger field results in an increase of the transverse velocity component.

Charged particle motion can be affected by the presence of the instruments used for measurements. When a metallic object is put into a plasma medium such as is found in the magnetosphere, it will be surrounded by what is known as a plasma sheath. When the plasma comes into contact with a material body, a contact potential is formed between the plasma and the body; therefore a voltage drop will exist across it. This is evidence of the strong tendency of a plasma to remain electrically neutral. Strong electrostatic forces act in balancing the positive and negative space charge in each volume element of the plasma. By studying the particle intensities and currents, the resultant net charge and equilibrium potential of a metallic object immersed in a plasma may be determined as well as the thickness of the sheath which is formed. Since the electrons have much greater random speed than the positive ions, the ion current density is neglected and the random electron current density is taken to be

$$j_e = \frac{Nev_e}{4} \tag{36}$$

where N is the electron number density, v_e is the electron velocity and e is the electron charge.

Knowing j_e it is possible to postulate that when an isolated metallic body is brought into the plasma, the electron current to the body is initially much greater than the ion current. From this we can deduce that the body will be charged negatively until the potential is lowered sufficiently so that the net charge arriving at the body is zero.

For the equilibrium condition to exist, an equal number of negative and positive charges must arrive at the body per unit time (no net current can flow to the body). Thus, in the equilibrium state, the plasma potential will be positive with respect to the body.

The concept of the Debye length or Debye shielding distance is seen when we observe the effects of a negatively charged body put in a plasma. Plasma dynamics show that the plasma will form a shell or sheath of positive charge density beyond which the plasma is unaffected by the charged body. The depth of this sheath is the Debye length. In a similar manner a positively charged body would have a negative charge density sheath around it. Beyond the sheath there exist equal positive and negative charge densities, but within the sheath these are unequal.

The numerical value for the Debye length can be found from an approximate solution to Poisson's equation for a positive charge put in a plasma. The Boltzman factor $\exp(-W/kT)$ gives the probability of finding a charged particle in a region of potential energy W. The electron density is

$$N_e = N_o \exp\left(e\,\frac{\varphi-\varphi_o}{kT}\right) \tag{37}$$

where T is the absolute temperature of the plasma, k is the Boltzman constant, N_o is the electron density where $\varphi = \varphi_o$, φ_o is the plasma reference potential and φ is the local potential. The positive ion density is

$$N_i = N_o \exp\left(-e\,\frac{\varphi-\varphi_o}{kT}\right) \tag{38}$$

if N_o is also the positive ion density in a region of potential φ_o. Now solving Poisson's equation for φ :

$$\frac{1}{r^2}\,\frac{d}{dr}\left(r^2\,\frac{d\varphi}{dr}\right) = -\,\frac{1}{\varepsilon_o}\left(N_i e - N_e e\right) = \frac{2N_o e}{\varepsilon_o}\sinh\left(e\,\frac{\varphi-\varphi_o}{kT}\right) \tag{39}$$

Since the differential equation is non-linear, Reitz and Milford (1962) suggest an approximate solution when $kT > e\varphi$ of allowing $\sinh\left(\frac{e\varphi}{kT}\right) \approx (e\varphi/kT)$, thus

$$\frac{1}{r^2}\ \frac{d}{dr}\left(r^2\ \frac{d\varphi}{dr}\right) = \frac{2N_o e^2}{\epsilon_o kT}\ \left(\varphi-\varphi_o\right) \tag{40}$$

which has a solution

$$\varphi = \varphi_o + \frac{Q}{4\pi\epsilon_o r}\ \exp\left(-\frac{r}{h}\right) \tag{41}$$

where r is the distance from charge +Q and h = Debye length.

$$h = \sqrt{\frac{\epsilon_o kT}{2N_o e^2}} \tag{42}$$

It can be shown that the product of the Debye length and inter-particle spacing is proportional to the square root of the ratio of the mean kinetic and inter-particle potential energies. The electrons and ions will combine when their potential energies are greater than their kinetic energies. In the upper magnetosphere and interplanetary space, the Debye length is much greater than the average inter-particle spacing and the gases remain ionized with little recombination. This is not true at lower altitudes when the mean free paths are small.

Another parameter of the plasma is the Debye or plasma frequency. If we go from a plasma equilibrium condition to one where the electron density is disturbed, the disturbance in the density will oscillate with a frequency

$$\omega_P = \sqrt{\frac{4\pi Ne^2}{m}} \tag{43}$$

where N is the electron density. In the outer magnetosphere $\omega_P \sim 10^6$ cps and decreases with increasing altitude since N decreases (MacDonald, 1964).

An example of the application of these particle and plasma parameters in an actual case is the study of a charged particle trapped in the geomagnetic field. The motion of trapped particles such as those in the Van Allen radiation belts can be summarized by looking at the three components of motion which contribute to the resultant complex motion of the charged particle. It has previously been noted that a charged particle moves in a circle of radius $R = \frac{mv_\perp}{qB}$ with an angular frequency $\omega_c = \frac{qB}{m}$ where q (= Ze) is the particle charge, m is its mass and B is the magnetic field magnitude. In the Van Allen belts the distance to the center of the earth from the particle is much greater than the cyclotron radius R, determined by calculation.

If the guiding center of the particle has a velocity vector which makes an angle α with the magnetic field direction at a position where the field strength is changing, it moves nearly parallel to the field line to a position where the field strength is $B_m = B/\sin^2 \alpha$ (B_m is the maximum field strength to which the particle can penetrate before it turns back along the field line; this is referred to as a mirror point) (Dessler, 1961). The Van Allen particles will thus travel between the northern and southern hemisphere mirror points, moving nearly parallel to the $\overline{B}$ field lines.

Along with the above motion, it is found that the particle has a drift velocity longitudinally, so that the negative particles drift eastward while positive particles drift westward.

If the particle were in a perfect dipole field, the guiding center of the particles would trace out a surface identical to that formed by the revolution of the magnetic field lines defined by

$$r = R_e \cos^2 \phi_m \qquad (44)$$

where r = geocentric distance to a point on the magnetic field line, ϕ_m is the magnetic latitude and R_e is the geocentric distance at which the field line crosses the equatorial plane.

For the non-perfect dipole fields, invariants are used to further describe the motion. The adiabatic (magnetic moment) invariant mentioned earlier is

$$\mu = 1/2\ mv_{\perp}^2/B \tag{45}$$

where m is the particle mass, $v_{\perp}$ the velocity component perpendicular to the local magnetic field direction and B is the magnitude of the magnetic field strength. μ stays constant provided the magnetic field strength changes only slightly over the distance the particle moves in one cyclotron period.

Another invariant is the integral (longitudinal) invariant and is given by

$$J = \oint m\bar{v}_{\parallel} \cdot d\bar{\ell} \tag{46}$$

This integral is taken over the mirror points with $\bar{v}_{\parallel}$ being the velocity component parallel to $d\bar{\ell}$, a line element along a force line. Thus if a particle moves with J and μ remaining constant, it must eventually drift back to the field line where it started.

The flux invariant is determined by

$$\phi = \int_s \bar{B} \cdot \bar{n}\ ds \tag{47}$$

where s is the integral invariant surface previously described. This integral is evaluated over a surface joining the magnetic equator at the surface of the earth to the integral invariant surface. If the geomagnetic field changes as in storms (when the magnetosphere contracts, then expands) this integral invariant surface will change so ϕ remains constant

along with J and μ. The resultant effect on the particle motion is that it follows the slow movements of the magnetic field.

c. Trapped Radiation Zones. At the earth's surface, radiation flux measurements are usually lower than those made on satellites and rockets since the earth's atmosphere partially shields the earth from the incoming radiation. For this reason little knowledge of the high altitude trapped radiation had been gained before the first satellites were put into orbit. Even since that time, problems have arisen concerning the measurement of these particle fluxes in that their spatial distribution is often quite complex and varied which makes it difficult to map the fluxes. It is also difficult to determine what part of the flux is from artificial sources such as high altitude nuclear explosions and which of it is of natural origin.

Naturally occurring trapped particles in the geomagnetic field with energies greater than 1000 ev are termed Van Allen radiation. Excluded from this category are the solar wind and the cosmic rays which cannot be explicitly designated as trapped radiation. Van Allen (1959) had detectors on Explorer satellites I, III and IV, which detected electron fluxes of energies greater than 3 Mev and proton fluxes greater than 30 Mev. These experiments and others showed the existence of belts of trapped particles now known as the Van Allen Zones.

The concept of trapped particle motion has been discussed previously and it applies in this case. The particles not only bounce from one hemisphere to another, but they also have a longitudinal drift caused by a $\overline{\text{grad}}$ B change over a cyclotron radius and also from the curving field lines which produce a centripetal force as the guiding center follows the field line.

Prior to the U.S. Starfish high altitude nuclear explosion of

July 9, 1962, and the three Soviet high altitude explosions of October 22, October 28, and November 1, 1962, there had been few measurements of particle fluxes in the radiation zones, particularly near L = 1.5 R_e (McIlwain, 1960). This presents a problem to experimenters when they try to determine what percentage of the trapped particles have been artificially injected. Some indication of this can be had by repeated measurements of the fluxes at one location and determination of the decay rate of what must be injected radiation since the naturally occurring radiation is assumed to be relatively constant.

Van Allen, McIlwain and Ludwig (1959) reported that Explorer IV data indicated an inner zone of high energy protons centered at approximately 1.5 R_e. Nuclear emulsions used in rocket flights by Freden and White (1959) showed tracks which confirmed this. Detectors flown on Explorer XV by McIlwain (1963) indicated a peak in the proton ($40 \leq E_p \leq 110$ Mev) flux at L = 1.5 R_e of $\sim 10^4$ protons/cm^2-sec and also a secondary peak at equatorial latitudes at 2.2 R_e of $\sim 5 \times 10^3$ protons/cm^2-sec. The secondary peak was not present in previous measurements of protons with energies less than 25 Mev. It appears that most of the protons are of natural origin since the fluxes remained nearly constant before and after the high altitude explosions. Magnetic storms cause only small, temporary changes in the proton flux.

Electron detectors have also been flown in the trapped radiation regions and the results indicate that many of the electrons have been artificially introduced. McIlwain's (1963) data from detectors on Explorer XV indicated that for electrons with $E_e \geq 5$ Mev there was a particle flux of $\sim 10^7$ electrons/cm^2-sec at L $\sim$ 1.4 R_e with a second peak of 5×10^5 electrons/cm^2-sec at L $\sim$ 1.7 R_e in the equatorial plane. It is felt that the electrons at L < 1.7 R_e were caused by the Starfish explosions while those

at $L > 1.7\ R_e$ were due to the Soviet explosions. Only one peak was found for electrons with $E_e \geq 0.5$ Mev and this was a flux of $\sim 10^9$ electrons/cm^2-sec at $L \sim 1.4\ R_e$. It is expected to be more than 20 years before the decay has been sufficient for these regions to return to near their pre-explosion condition which will allow more precise determination of the particle fluxes.

It has been postulated that the albedo-neutron mechanism for decay accounts for the protons and electrons trapped in the Van Allen belt (Freden and White, 1960). This theory states that neutrons produced by high energy cosmic ray collisions in the atmosphere leak into space and decay. Some of the protons and electrons from the above process are trapped and thus form the radiation belt. Once trapped, they spiral about the magnetic field lines and are reflected at the mirror points in the two hemispheres. The particles remain trapped until they are removed by various loss mechanisms.

d. Cosmic and Solar Radiation. In further describing the medium in which the electric field measurements will take place, it is necessary to mention cosmic and solar radiation. Cosmic rays are photons and atomic nuclei from outside the earth's atmosphere with velocities in or near the relativistic velocity range. Solar cosmic rays are believed to originate in the sun and are present in periods of a few days during high intensity radiation activity on the sun. Their maximum energy is about 20 - 30 Bev. Other cosmic rays originating within our Galaxy are called galactic cosmic rays and consist mainly of hydrogen nuclei, protons and helium nuclei (α particles). The sources of solar cosmic rays are stars (such as the sun), novae and supernovae, plus more than 50 extra-galactic sources which have been observed.

The cosmic ray flux has not varied appreciably over long periods of time, but there has been, however, experimental evidence of an eleven-year cycle in which the intensity increases as solar activity decreases. Temporary large-scale reductions take place and are related to magnetic storms in which it is believed that the $\overline{B}$ field carried by the solar wind plasma shields the earth from the cosmic rays. These are known as Forbush decreases.

During solar minimum the energy flux of cosmic rays is about 1400 Mev/cm^2-sec-sterad in the free space about the earth. This is similar to the energy delivered to the earth by starlight. The intensity curve is reasonably flat and has limits at 10^3 particles/m^2-sec-sterad for 10^{16} ev (energy per nucleon) particles and 10^{-14} particles/m^2-sec-sterad for 10^{19} ev particles (Rosen and Vogl, 1964)

One other source of penetrating radiation is from solar flares which eject high energy protons and electrons. Proton energies near 200 Mev have been detected near the polar regions inside the auroral zones half an hour or more after large solar flares appear. The radiation gradually diminishes over a period of several days. For large flares the proton flux is on the order of 10^{14} protons/cm^2-sec and for smaller ones it is near 10^2 protons/cm^2-sec. In general, it appears that solar and cosmic radiation intensities are too low to have an appreciable effect on the type of probe measurements discussed in this paper.

e. The Earth's Magnetic Field. It is necessary to know the $\overline{B}$ field at every point during the flight for accurate measurements of the electric field (due to $\overline{v} \times \overline{B}$ effects discussed later). A brief description of the earth's magnetic field will now be given. A first approximation of the earth's magnetic field is that of a magnetic dipole

located at the center of the earth. The magnitude of the $\bar{B}$ field is then calculated at a distance r(cm) from the center of the earth by

$$B = \nabla \left(\frac{\mu \cos\theta}{r^2} \right) \tag{48}$$

where μ is the magnetic moment of the dipole (gauss/cm^3) and θ is the colatitude (Cahill, 1964). The approximation grows worse as r decreases due to sources such as ores near the earth's surface. The ordinary variations of the surface field are less than one per cent and only become larger during magnetic storms when there may be variations of one to two per cent.

The main component of the earth's magnetic field is believed due to dynamo action in the fluid motion of the molten metallic core of the earth (Elsasser, 1950). Since the fluid motion is not stable, it changes slightly from year to year and thus produces a secular variation taking hundreds of years to produce a significant change in the magnetic field. Shorter (1 year and under) variations are produced primarily by interactions between solar plasma and the geomagnetic field. Elsasser's theory (1950) requires the dynamo system to have large linear dimensions resulting in slow current decay and an angular velocity large enough to produce a coriolis force to provide a current feedback loop. Initially, there must be a driving energy source to cause the motion.

Variometers are used to make continuous recordings of the components of the field at ground stations. Both suspended magnet and precession instruments are in common use. By correlation of these

readings at various points on the earth's surface, magnetic maps can be plotted. Several types of variations are recorded and should be mentioned. The S_q variation with a period of 1 solar day is apparent on magnetically quiet days. This is less noticeable on days of magnetic storms when the disturbance daily variation, S_D, is large. The diurnal amplitude depends also on the time during the 11-year solar cycle and the solar year.

Superimposed on S_q is L, the lunar daily variation. During stormy periods there are many short variations which have no regular pattern. Both the S_q and L variations are caused by electric currents flowing in the ionized regions of the atmosphere while the S_D variations are due to a ring current at several R_e and to electric currents at the boundary of the magnetosphere (Cahill, 1964). The magnetosphere is shaped by the pressure of the solar wind and when this fluctuates, hydromagnetic waves are set up which are observed as small fluctuations on the earth's surface. Certain other variations are due to auroral fluctuations and other low frequency phenomena.

In recent years both satellite and rocket-borne magnetometers have been used in the study of the $\overline{B}$ field and ring current. Through such measurements a knowledge of the magnetosphere boundary and interior of the magnetosphere has been obtained with increasing accuracy. Near the equator the surface $\overline{B}$ field has a magnitude of about 0.3 gauss while at auroral latitudes it is nearer 0.5 gauss. Just outside the boundary of the magnetosphere on the sunlit side of the $\overline{B}$ field in the equatorial plane as measured by Explorer XII was approximately 30 gammas while inside the boundary it is close to 100 gammas (Cahill, 1963). In electric field measurements it is suggested that two or three component

magnetometers be used simultaneously to provide accurate $\overline{B}$ field information to allow the calculation and correction for the $\overline{v} \times \overline{B}$ error in the measured electric field.

2. Theory and Technique of Probe Measurements

The technique proposed in this thesis for making electric field measurements in space can be briefly summarized. Since there have been disturbing effects when the probes have been flush mounted on the vehicle due to the vehicle plasma sheath, it is suggested that the conducting probe areas be held away from the vehicle body on booms which will be extended automatically after the vehicle is out of the dense atmosphere. Each boom will be electrically connected to a very high input impedance ($\sim 10^9$ to 10^{11} ohms) field effect transistor electrometer differential amplifier which detects the potential difference between the two probes by monitoring the small current flow through a high impedance between them. The output from the electrometer amplifier is then applied to a subcarrier oscillator. The voltage variations are converted into frequency variations which are then transmitted to receiving equipment on the ground. The method of data handling and transmission depends, of course, on the specific experiment but the initial probe-electrometer amplifier stages remain essentially the same. It is with this experimental concept in mind that one can look, with more detail, at the detector stages of this technique.

The concept of collecting small currents with conducting probes in a plasma appears straightforward but is actually of a complicated nature when the many possible effects that can take place are considered. Some of these which can lead to considerable error in the electric field measurements will be considered here. Some effects

such as those caused by the RF fields due to telemetry and by secondary emission of electrons are small enough or at high enough frequency to be considered negligible and won't be discussed further.

The first topic is the equilibrium potential of conducting bodies in a plasma. There have been studies of the equilibrium potential of satellites by Bourdeau et al. (1961) on Explorer VIII and by Kurt and Moroz (1962) on the Soviet space rockets. For simplicity, due to symmetry, it is clearest to discuss these effects using the model of a conducting sphere in a plasma medium.

Although a metallic sphere immersed in a plasma can become positively charged, it is more likely that it will acquire a negative potential due to the higher velocity of the electrons. It is for this reason that only a negatively charged sphere is considered here although a similar analysis can be used for a positively charged sphere.

The random electron current density to a negatively charged sphere is given by (Langmuir, 1926)

$$J_e = - j_e \exp\left(\frac{e\varphi}{kT_e}\right) \tag{49}$$

where e is the elementary charge (coulombs), k is Boltzman's constant (Joule/^oK), T_e is the ambient electron temperature (^oK) and φ is the potential (volts). The expression for j_e is

$$j_e = \frac{N_e e v_e}{4} \tag{50}$$

where N_e is the electron density (electrons/m^3), and v_e is the mean thermal electron velocity (m/sec) which is evaluated (assuming a Maxwellian distribution) as

$$v_e = \sqrt{\frac{8kT_e}{\pi m_e}} \tag{51}$$

where m_e is the electron mass (kg). The negative current is found by taking the surface integral of J_e over the sphere surface.

The ion current density to a negatively charged sphere has also been given by Langmuir (1926) as

$$J_+ = j_+ \left[1 - \frac{a^2 - r^2}{a^2} \left(\exp \left[- \frac{r^2}{a^2 - r^2} \cdot \frac{e\varphi}{kT_+} \right] \right) \right] \qquad (52)$$

where φ is the equilibrium potential (volts), T_+ is the ion temperature, r is the sphere radius (m), and a is the outer radius of the plasma sheath (m) and is given by

$$a = \lambda_D \sqrt{\frac{- e\varphi}{kT_e}} + r \qquad (53)$$

where λ_D is the Debye length and φ is negative. In the equation for J_+ the expression for j_+ is

$$j_+ = \frac{N_+ e v_+}{4} \qquad (54)$$

where N_+ is the ion density (ions/m^3) and v_+ is the mean ion velocity which is given by

$$v_+ = \sqrt{\frac{8kT_+}{\pi m_+}} \qquad (55)$$

when $r \gg (a-r)$, J_+ can be approximated by

$$J_+ \approx N_+ e \sqrt{\frac{kT_+}{2\pi m_+}} \qquad (56)$$

The positive current to the sphere is found by taking the surface integral of J_+ over the plasma sheath surface.

Since the speed of the ion is $(m_e/m_+)^{1/2}$ (m_e is the electron mass and m_+ is the ion mass in kg) times smaller than the speed of the electron one expects that $J_e \gg J_+$, a larger electron current than ion current

flows to the sphere. As a result, an initially uncharged sphere becomes negatively charged and has a positive ion sheath.

In cases where sunlight falls on the sphere, there will be a photoelectric emission current density J_{ph} which has been evaluated by Hinteregger (1959) as

$$J_{ph} \sim .5 \times 10^{-5} \text{ amps/m}^2 \tag{57}$$

where the integral for the photoelectric current is taken over the sphere surface.

In an equilibrium condition the net current flow to the sphere must be zero thus a current balance equation can be written

$$\int J_e \, ds + \int J_+ ds + \int J_{ph} \, ds = 0 \tag{58}$$

The equilibrium potential may be obtained by solution of this equation

$$- j_e \exp\left(\frac{e\varphi_o}{kT_e}\right) S + \int J_+ ds + \int J_{ph} \, ds = 0 \tag{59}$$

After dividing by j_e S and taking the Ln

$$\frac{e\varphi_o}{kT_e} = \text{Ln} \left[\frac{\int J_+ ds + \int J_{ph} \, ds}{j_e S} \right] \tag{60}$$

therefore

$$\varphi_o = - \frac{kT_e}{e} \text{ Ln} \left[\frac{j_e S}{\int J_+ ds + \int J_{ph} ds} \right] \tag{61}$$

where e = 1.60×10^{-19} coulombs and φ_o is the floating potential (volts) of the sphere with respect to the plasma. A rough calculation of the potential with T = 10^3 ^oK, $N_e = N_+ \approx 10^{11}$ particles/m^3 appropriate to the ionosphere (neglecting J_{ph}), gives $\varphi_o \approx$ - .32 volts.

If the sphere is moving in a magnetic field or if a potential gradient exists in the plasma, the net current to a surface element ds may not be zero yet the total current to the sphere will be zero for an equilibrium situation. The ion and electron current to a spherical probe (not in the sunlight) can easily be calculated for various altitudes. It is found at 80 km the net equilibrium electron and positive ion current to a probe with a 10 cm radius with $N_e = N_+ = 10^9$ particles/m^3 and at $T = 200^oK$ with an equilibrium potential of $\varphi_o = -.06$ volts is $\sim 1.32 \times 10^{-8}$ amps. In an actual application where the potential difference is measured between two probes the measuring electrometer will draw about 10^{-9} to 10^{-11} amps when $|\varphi_o| \sim 1$ volt. The error analysis in a later section will show the approximate error in the measurement of the potential difference caused by this leakage current.

In the case where the probe moves through a plasma, Bourdeau et al. (1961) have made measurements on Explorer VIII that indicate the ion current is strongly dependent on the probe velocity relative to the plasma. The ion current was measured on Explorer VIII and plotted as a function of the velocity azimuth angle (θ). The ion current was found to rise from low values ($\sim 10^{-12}$ amps) for θ near 180^o to values of 2.5×10^{-10} amps for θ near 0^o at an altitude of 1000 km. From this one can conclude that the very low ion current (due to low ion velocities) on the side away from the velocity vector is indirect evidence of a negative wake. The probe is surrounded by a positive sheath which has λ_D (Debye length) thickness on the front side and surrounds the wake on the back. This increase in ion current is reasonable since the ion thermal velocity is comparable to the probe velocity for satellite and rocket applications thus resulting in a "pile up" of positive ions on the velocity vector side of the probe and an absence of positive ions on the other side.

Since the electron thermal velocities are much higher, there is no noticeable increase in the electron current to the probe. Sagalyn et al. (1963) treat this by assuming that the ion trajectories are not influenced by the local electric fields around the probe. Fahleson (1966) uses an approximation to Sagalyn's equation

$$I_+ \approx \pi r^2 N_+ e \sqrt{\frac{8kT_+}{\pi m_+} + v^2} \tag{62}$$

where v is the velocity of the sphere relative to the plasma (m/sec). In the Explorer VIII measurements Bourdeau et al. (1961) also found that the electron current reached a maximum when the detector was facing the sun due to the additional photo-emission current.

If we take all of these effects into account and assume that $r \gg a\text{-}r$, the preceding equations can be combined and solved for the probe potential with respect to the plasma (Appendix A).

$$\varphi = \frac{-kT_e}{e} \operatorname{Ln}\left[\frac{\sqrt{\frac{kT_e}{2\pi m_e}}}{\left(\frac{N_+ S_p}{N_e S}\right)\sqrt{\frac{8kT_+}{\pi m_+} + v^2} + \left(\frac{S_p}{S}\right)\frac{J_{ph}}{N_e e} - \frac{I}{SN_e e}}\right] \tag{63}$$

where I is the leakage current of the measuring instrument (amps), S is the surface area (m^2), S_p the projected area (m^2) and $e = 1.60 \times 10^{-19}$ coulombs. If I is set equal to zero the floating potential φ_o is obtained. S_p for J_{ph} and J_+ may be different for a non-spherical object.

It has been previously mentioned that the motion of a sphere (or conducting probes) through a plasma in the presence of a magnetic field $\bar{B}$ will cause an induced $\bar{v} \times \bar{B}$ field which must be considered in the electric field measurements. The induced field will change the potential of the

probe with respect to the surrounding plasma. In the case of two probe systems, this leads to an error in measurement of the potential difference created by the electric field in the plasma. This error can be calculated if the probe velocity with respect to the $\overline{B}$ field is known.

Bourdeau (1961) and Aggson and Heppner (1965) suggest that the $\overline{v} \times \overline{B}$ field and zero net current condition will cause a redistribution of the polarity of the charge distribution on non-spherical probes similar to that measured on Explorer VIII (Bourdeau, 1961). For cylindrical booms this would indicate that one end of the boom would have a positive potential allowing the electrons necessary for equilibrium to be collected. The remainder of the boom is in an electron depleted sheath where it collects only ions and thus assumes a non-uniform floating potential relative to the plasma and dependent on d, the distance between probe centers. Beard and Johnson (1960) find that a metallic satellite moving across the earth's magnetic field will develop a potential per unit length perpendicular to the field of 10^{-8} Bv (volts/cm) where B is in gauss and the velocity (v) is in (cm/sec). This induced potential has a negligible effect on the ion motion because of their heavier mass, but will influence the electron current in such a way that it will be incident at the high potential end of the satellite. The ion current can be considered as uniform over the projected area of the vehicle perpendicular to the velocity while the electron current is incident at the end of higher potential. Since the electron thermal velocity is much greater than the satellite velocity the electron flux will be proportional to the average electron velocity while the ion flux will be proportional to the satellite velocity. Using the condition that there will be equal fluxes, it is seen that the area of electron incidence is proportional to the projected area of the satellite times the ratio of the satellite velocity to the electron

velocity. Since the electron velocity is large compared to the satellite velocity, the area of electron incidence will be a small part of the projected area.

For various trajectories and orbits the $\bar{v} \times \bar{B}$ effect can easily be calculated if the attitude of the probes is known with respect to the $\bar{B}$ field as well as the velocity of the vehicle and magnitude of the $\bar{B}$ field. These measurements must be made in conjunction with the proposed experiment; the accuracy of these measurements may limit the measurement of the electrostatic fields.

Considering the case of a satellite in an elliptical orbit with an orbit of $\sim 6\ R_E$, the $\bar{v} \times \bar{B}$ effect will be continuously changing due to the varying parameters. An example would be a satellite whose velocity at $5\ R_E$ might be 2.0 km/sec with a .2 radian angle with respect to a $\bar{B}$ field of 2.4×10^{-3} gauss. For a 20 meter probe separation the induced potential difference can be calculated from

$$\Delta\varphi = (\bar{v} \times \bar{B}) \cdot \bar{d} \tag{64}$$

where $\bar{v}$ (cm/sec) is vehicle velocity with respect to the $\bar{B}$ field lines, $\bar{B}$ is the magnetic field in webers/m^2 (1 w/m^2 = 10^4 gauss) and $\bar{d}$ is the probe to probe center point distance where $\bar{d}$ is taken parallel to $\bar{v} \times \bar{B}$. For the conditions described above $\Delta\varphi \approx 1.92$ mv. At a point closer to perigee the parameters might be $\bar{B} = 1.6 \times 10^{-2}$ gauss, $\bar{v}$ = 5 km/sec, and still using a 20 meter probe separation (to midpoint of each probe) and a .2 radian angle $\Delta\varphi \sim 32$ mv. It is seen that even if the angle remains the same, the other parameters result in a considerable change in the induced potential difference. In these calculations corotation of the earth's field lines with the earth has been assumed.

A satellite flown in a circular synchronous orbit should not have

a $\bar{v} \times \bar{B}$ effect due to the forward motion of the satellite since there will be no motion relative to the corotating $\bar{B}$ field. It is reasonable to expect, however, that areas of irregularities or hydromagnetic waves moving past the satellite could cause inductive "kicks". These would be random and presumably easily detected provided magnetometers were also being flown.

The $\bar{v} \times \bar{B}$ effect can also be easily calculated for a rocket which is not precessing. For the case with two symmetric probes extending perpendicular to the axis, it will be seen that the potential difference ($\Delta\varphi$) between the probes is

$$\Delta\varphi = (\bar{E} + \bar{v} \times \bar{B}) \cdot \bar{d} \tag{65}$$

where $\bar{d}$ is the distance of separation of the midpoints of the probes. The potential difference $\Delta\varphi$ between points $\bar{\ell}_2$ and $\bar{\ell}_1$ is defined as

$$\Delta\varphi \equiv \int_{\bar{\ell}_1}^{\bar{\ell}_2} \bar{E}' \cdot d\bar{\ell} \tag{66}$$

where in the present case there are two $\bar{E}$ fields to consider; that due to the electrostatic $\bar{E}$ field and that due to the induced $(\bar{v} \times \bar{B})$ field. Thus it is seen that

$$\Delta\varphi = \bar{E}' \cdot (\bar{\ell}_1 - \bar{\ell}_2) = (\bar{E} + \bar{v} \times \bar{B}) \cdot (\bar{\ell}_1 - \bar{\ell}_2) \tag{67}$$

where $(\bar{\ell}_1 - \bar{\ell}_2)$ is the separation of the midpoints of the probes.

If the rocket is not spinning or precessing, one would expect to measure the electric field potential difference between the probes plus the slowly changing potential differences due to the $\bar{v} \times \bar{B}$ effect. If, as in most cases, the rocket is spinning, the resultant potential differ-

ence will vary as a sum of two cosine terms. This is seen in Figure (6) where the resultant $\Delta\varphi$ is measured by an electrometer amplifier between the two probes. The $\Delta\varphi_o$ term is due to the original electric field present (assumed constant here) and is given by

$$\Delta\varphi_o = E\, d \cos(\bar{d}, \bar{E}) \tag{68}$$

where d is the probe separation and E is the electric field. The term caused by the forward motion of the rocket is

$$\Delta\varphi_1 = v\, B\, d \sin(\bar{v}, \bar{B}) \cos(\bar{v} \times \bar{B}, \bar{d}) \tag{69}$$

where $\bar{v}$ is the velocity of the probes relative to the plasma. One might expect a third term due to the rotational motion of the probes about the spin axis where the spin vector, $\bar{\omega}$, is assumed perpendicular to $\bar{d}$. It is quickly seen, however, that the $\bar{v} \times \bar{B}$ fields of the two probes are opposed and thus one would expect there would be no potential difference created by the rocket spin. The total potential difference between the midpoints of the probes is then $\Delta\varphi = \Delta\varphi_o + \Delta\varphi_1$ and knowing the separation, d, the electric field can be calculated as

$$|E| = \frac{\Delta\varphi}{d} \tag{70}$$

where $\Delta\varphi$ is the potential difference corrected for $\bar{v} \times \bar{B}$ (volts/m), and d is the probe separation (meters).

In the auroral zone (100-120 km) it is estimated the $\bar{E}$ fields are on the order of 10 to 100 mv/m. As an example of the magnitude of the potential differences $\Delta\varphi_o$ and $\Delta\varphi_1$, we can assume a collinear probe system with separation d of 2 meters and a velocity of 2 km/sec at an angle of .5 radian to a .4 gauss $\bar{B}$ field. The calculated potential difference due to the $\bar{v} \times \bar{B}$ effect is $\approx$ 77 mv while the $\bar{E}$ field potential difference is

$\approx$ 20 to 200 mv assuming an $\overline{E}$ field of 10 to 100 mv/m. It is seen that $\Delta\varphi_1$ potential must be calculated accurately if reasonable accuracy in the $\overline{E}$ field measurements is desired.

For a spinning rocket a full revolution is needed to find the peak values of the $\overline{E}$ field if the field is "static". It is for this reason that the spin rate should be high enough to avoid traversing a large distance before one measurement cycle is completed unless the field itself is oscillating at the same frequency. Allowing the probes to rotate enables both magnitude and vector field measurements as well as eliminating the problems involved in D.C. voltage measurements such as amplifier drift and contact potential errors. Of course, only the $\overline{E}$ component perpendicular to the spin axis will be measured. A spin rate which is too high creates problems in that the bandwidth of the electrometer must be larger which leads to increasing thermal noise voltage.

$$V_T = \sqrt{4kTAR} \tag{71}$$

where T (^{o}K) is the temperature of the resistance, R (ohms) between the probes, and A (cycles/sec) is the bandwidth of the amplifier. The resistance between the probes can be made less than 10" ohms and will be adjusted as required in a specific experiment.

SECTION IV

THE ELECTRIC FIELD METER AND PROPOSED ROCKET EXPERIMENT

1. The Probe System

The first flight test of the electric field meter described in this paper will be on a sounding rocket passing through an auroral display (~100-120 km). Calculations show that the Debye length in this region is on the order of .01 meters while the particle mean free path is approximately 1 meter. In order to avoid a sheath overlap between the rocket sheath and the probe sheath, it is desirable to have the probes at least .01 meters away from the rocket body. This is easily accomplished at lower altitudes but is increasingly difficult for satellite applications at higher altitudes where λ_D becomes much larger (i.e. $\lambda_D \sim 40$ m at 50,000 km) and the booms holding the probes must be quite long. For this specific application, however, it is seen that reasonably short booms can be used. Another criteria of the probe separation is that they be separated at a distance greater than the mean free path of the electrons and ions whenever possible in order that meaningful results can be obtained. Once again, this would represent a serious problem at 50,000 km where the mean free path is $\sim 10^8$ m. At rocket altitudes this presents no particular problem since the mean free path is near one meter.

For all applications using the electric field meter, it is best to have the probes symmetrically mounted so that the exact distance between the centers is always known. For rocket applications

symmetrical probes are a necessity if rocket precession is not desired. Other general requirements for the probe system are that the probes and connections be electrically identical to prevent errors due to contact potentials. The booms must be extended after the rocket is above the atmosphere to avoid drag effects. Since the rocket has a speed of about 1525 m/sec at 100 km, it is necessary that the deployment of the booms take only a few seconds to avoid traveling through the principal auroral zone of interest at 100 to 200 km without making measurements. It is planned to deploy the booms after burnout which occurs at approximately 17 km and well before 100 km.

The rocket (a Nike-Apache or Nike-Tomahawk) to be used is carrying a large number of experiments. Therefore, it is felt that the lightest and least complex boom and probe arrangement is desirable. Since the electric fields at this latitude and altitude are believed to be primarily horizontal, it is desirable to measure the horizontal component of the electric field. This requires the booms to extend perpendicular to the payload center axis. With these requirements in mind, it was decided to forgo the standard, heavier and more complex mechanical fold-out booms in favor of a new style of boom which is beginning to be used widely in the field of space physics. The booms to be used on this experiment are of the unfurlable type, made of copper beryllium, titanium or stainless steel. They are lightweight (.01 pound/ft. for .3 inch radius titanium) and have the form of a tube with a cylindrical cross section when extended. Before extension they are stored on drums or wrapped together about the payload body - similar to tape stored on a reel. When released they have a potential energy great enough that they extend by themselves into the resulting cylindrical form.

The deployment is made after the rocket has left the dense atmosphere so that air drag will have little effect. Calculations show that the spin rate will be reduced by approximately 30%, but this should not affect the rocket stability, and the rocket is not expected to precess about its spin axis. To prevent precession the booms must be extended simultaneously.

Several methods of deployment are possible. In one case the booms can be wrapped overlapping on an internal motor-driven drum which then feeds them out at a controlled rate. Another method is to wrap the booms externally about the payload. If they are wrapped overlapped and if their bases are mounted at opposite points on the payload, they will extend simultaneously by themselves when released. Since the booms will not have to be retracted, this is felt to be the most reliable method of deployment and the least complicated. The booms, when wrapped around the rocket, will be protected by a spring-loaded shroud which will be flung off when set free by a pyrotechnic pin puller. In the extended position there is a sizeable restoring force which should cause the booms to come to an equilibrium extended position in a relatively short time.

The probe will actually be part of the boom in that it is made of a conducting metal. Each boom length will be approximately five feet long with the inner half insulated by a thin coating of Teflon or varnish. The outer two and a half feet will be the conducting probe section and the boom itself will be the electrical conductor to the base connections into the electrometer. Since the input impedance of the electrometer is on the order of 10^{10} ohms, the booms must be well insulated from each other and from payload structure.

Various suppliers have been contacted, and Ryan Aircraft of San Diego, California, is working on the fabrication of the booms for this experiment.

There are other boom configurations which can be used, such as an X array of booms to eliminate unwanted effects from shadowing, and booms mounted symmetrically at various angles to the rocket axis to measure different components of the field. In later measurements it is expected that several probe systems can be used simultaneously to provide a three-component measurement of the electric field.

2. Differential Electrometer Amplifier

The requirements for an electric field meter have been stated in previous sections of the paper, but it will be beneficial to restate them here. The meter must have a high input impedance on the order of 10^{10} ohms and be capable of measuring millivolt signals while drawing only a minimal current ($\sim 10^{-11}$ amps). Since it will be used in rocket and satellite applications it should not require an unusually high power supply voltage or power, and it must be fairly stable with temperature variations. Temperature stabilization and the range needed can be designed in the instrument once exact specifications are set, but for the present time, a meter which can measure the small potential difference while drawing a small current is desired. The art of measuring electric fields in space is just developing and as a result there were few previous circuits of this exact nature to gain experience from. A summary of those and the final circuit are given in this section.

Keithley Instruments of Cleveland, Ohio, has designed electrometers of this type for rocket and satellite use which use electrometer

vacuum tubes for the dual input stages. It was felt, however, that an electric field meter designed with entirely solid state components would be superior for both rocket and satellite use due to the stability against shock and vibration and the low power requirements.

NPN and PNP junction transistors were considered for the dual inputs (one for each probe) but the input impedance of these devices is much too low for successful application and this idea was soon abandoned. Since it was desired to measure a potential difference between the probes and not the floating potential of them, a differential amplifier was immediately considered as the basic circuit. The only solid state devices with a high enough input impedance to be used in the initial amplifier stages of the circuit were the newly developed field effect transistors. These devices act as current gates and they can control the current flowing between the drain and source when a small voltage is applied to the gate. Although only small currents are drawn through the gate, the space charge about the gate will determine the current flow between the drain and source by effectively narrowing or broading the current channel.

Aggson and Heppner (1965) have proposed using a circuit built by Washington Technological Associates which employs a preamplifier with dual FET's (field effect transistors) which lead into a differential amplifier. A circuit similar to this was constructed during the early stages of the research for the meter described here and several circuitry techniques were learned from it. Several books were also consulted in the design stages of this instrument (Hurley, 1958; Sevin, 1965; and others listed in the references) as well as numerous specification sheets supplied by the various component manufacturers.

As the design research progressed, several different circuits were constructed and tested to see what was the best circuit for the criteria listed. Often a circuit would have one outstanding feature such as a high input impedance yet would fail to meet the specifications due to some fault such as low gain. By working with several circuits it was felt that the best points could be taken from each and combined into a circuit which would be satisfactory. It is felt by the author that such a circuit has finally been achieved.

The final circuit is of the operational amplifier type discussed by Sevin (1965) and Gosling (1965). It is of a unique class of differential amplifiers in which high impedance input FET's are actually used in each side of the differential amplifier. Not only does this decrease the number of components but it also reduces the power requirements of the instrument and improves the temperature stability.

From the schematic (Figure 15) it is seen that the differential input from the probes is fed directly into the gates of the FET's (Motorola MM2103). Thus a small millivolt potential difference exists across these inputs when the collinear probes are parallel to an electric field. As mentioned earlier, the gates have a high input impedance thus only a small current will flow from the probes. The error caused by this probe current leakage is analyzed in part 6 of this section. The FET's are the basis of the differential amplifier in that the gate of one will be at a higher or lower potential than the other. The result of this is that one FET will turn on (i.e. allow a higher current flow between the drain and source) while the other turns off. Since only the potential difference has an effect, this section of the circuit is thus referred to as a differential amplifier. Since the differential section is obviously

dependent on symmetry both of the FET's should have matched characteristics and R_1, R_2, the current limiting resistors, should be similar to within ± 1%. Temperature variations of current in a symmetrical circuit such as this tend to cancel which is desirable. The inputs are further stabilized by the constant current source composed of the 2N726 transistor and current limiting emitter resistor R_{13}. R_{12} is a bias resistor into the base and for a higher emitter collector current flow 2N726 tends to turn off and for a smaller current flow it turns on thus providing a constant current source. R_{11} is also a biasing resistor which completes the current path between + 12.0 volts and ground.

At point A the current will increase and decrease relative to the zero input state. The variations are used to bias the 2N735 transistor on and off depending on the input signal. R_3 is the emitter current limiter at this stage of the circuit. Since the input can go plus and minus it is desirable that the output do the same. For this reason R_3, R_4 and R_5, R_6, R_7, R_9, R_{10} are used to set the level of the output between ± 12.0 v.

Transistor 2N726 with R_5, R_6 as emitter current limiters acts as a reference with respect to ground since it is biased by R_8 and R_{14} similar to the other 2N726 transistor current supply. Thus point B can go positive and negative with respect to a set level. This in turn acts as a variable biasing for the 2N1132 transistor in the final stage of the output. As 2N1132 turns on and off the emitter level varies with respect to ground. The output can go positive and negative with respect to circuit ground since the level is set between the + 12 and - 12 volt power supplies by the current flow through the emitter resistors of the 2N1132. The zero input, output level is thus adjusted by varying the emitter resistances as shown. The voltage gain of the circuit described is

approximately 80.

The instrument described above has been tested, and the results are discussed in part 5 of this section. Before the circuit is actually used, certain changes may be made such as adding thermistors to control temperature variations, changing FET's to increase the input impedance or using capacitance to limit the frequency response to a smaller bandwidth or to prevent oscillations. These changes however will be of a minor nature, and the general circuit design will remain the same.

The power requirements are well within the range allowed on most satellites and rockets. At + 100 mv input the power requirements for the $\pm$ 12.0 volt power supplies are $\sim$ 30 miliwatts. At - 100 mv the power requirement is $\sim$ 18 milliwatts.

Since the circuit consists of entirely solid state components the packaging is expected to present no unusual problem. Printed circuit boards will probably be used and the circuit may be placed in a mu metal or copper box to provide magnetic shielding for the magnetometers on the rocket or satellite and/or RF shielding for the electrometer. It is likely that a potting resin will be used to guard the circuit from vibration and shock during launching.

3. Flight Calibration

The electric field meter has been tested in the lab under rather "ideal" conditions which are not always present on the launching pad and in flight. It is reasonable to expect that under these conditions the operating parameters of the instrument might drift from the "ideal" values. To insure the accuracy of the measurements, it is desirable to be able to check the operational accuracy and zero point of the electrometer differential amplifier by applying known millivolt potential

differences at regular intervals during the duration of the rocket flight.

The telemetry system subcarrier oscillators have an input range of 0 to + 5 volts. The electrometer amplifier has been designed with an output (which is fed into the subcarrier oscillators) of ± 2.5 volts with respect to the zero point D.C. output level (where the inputs have no potential difference applied between them). To make full use of the ± 2.5 volt output, the D.C. output level for grounded input is set at + 2.5 volts. In flight this D.C. level is important since it can shift the entire range of measurement by the amount that it drifts. Checking this level in flight is easily accomplished by using a relay to short out the two probes. The effect of the D.C. level change is seen in part 5 of this section (Testing).

Applying known potential differences can be accomplished in a similar way by using relays and standard cells. It is felt that the known potential difference calibration should be near the upper limits of the instrument since there is the zero point calibration at the midpoint of the instrument range. The electric field meter designed for this project has a range of ± 100 mv thus the calibration potentials will be on the order of ± 10 to 100 mv.

The actual switching techniques will have to be done using mechanical relays rather than solid state multivibrators. This is because the input impedance of the field effect transistors is much higher than that of the ordinary transistor thus making it impossible to use external electronic circuitry between the probes which is not completely disconnected by relays. Since the calibration signals will be applied at known time intervals, the data can be accordingly analyzed by comparing the data on the flight tape with a standard time signal.

4. Telemetry

An integral part of any rocket experiment is the telemetry system which transmits the data from the experiment to receiving stations on the ground. The telemetry system to be used has four main components, and they will briefly be described. These components are all flown on the rocket and are used in conjunction with the receiving instruments located on the ground. The general layout of the apparatus is seen in the block diagram (Figure 8).

The first stage after the electrometer differential amplifier is the subcarrier oscillator which converts the output voltage variations of the electrometer amplifier into frequency variations. As was mentioned earlier the input range is 0 to + 5 volts which produces a frequency deviation from the center frequency at which the subcarrier oscillator operates at when there is a + 2.5 volt input signal. Larger or smaller input voltages will thus produce a deviation from the center frequency.

When several experiments are flown on one rocket, several different subcarriers will be used. To avoid overlapping of frequencies between different subcarrier oscillators, the IRIG proportional bands 1- 21 will be used. Each band has a center frequency with a frequency band width equal to $\pm$ 7.5% of the center frequency. The center frequencies are chosen so that the lower limit of one band does not overlap the upper limit of an adjacent band. There are presently 21 bands with center frequencies running from 400 to 165,000 cps.

Since for most rocket flights there are several subcarrier oscillators, it is necessary to provide some kind of mixing network so that the various subcarrier outputs may be fed into the transmitter. This is accomplished by using a mixer amplifier which will combine the

outputs from the various subcarriers and amplify them so they may be fed as one signal into the transmitter.

The transmitter is a 2 watt F.M. output stabilized unit which operates at a frequency of 244.3 mc. The output of the transmitter is then fed into four whip antennas at the base of the payload section. Vector Telemetry of Los Angeles will be the supplier of the telemetry components, and the system integration and assembly will be done by the experimenters involved.

The ground receiving equipment is the standard type found at most rocket launching sites. The transmitted data is recorded on magnetic tape along with a time signal. To obtain the data from a specific experiment, the flight tape is played back with the output fed into discriminators and filters which select the experimental data desired. Once the data is obtained, it will be necessary to calculate the $\overline{v} \times \overline{B}$ effect which can be done using a program similar to the one shown in Appendix B. This was written by the author for the CDC 3600 computer to estimate what the $\overline{v} \times \overline{B}$ errors for various parameters in regions of the ionosphere might be. Further programs to plot the data and to calculate the $\overline{E}$ field will be written to expedite the data handling and analysis.

5. Testing

Several tests have been made on the electric field meter discussed in this thesis and the results will be discussed here. For a given output voltage from the instrument there must be some way of telling what the differential input voltage is. This can be done with the "ideal case" calibration graph shown in Figure 9. The "ideal case" refers to operating conditions where the power supplies were operating at the + 12.0 v. and - 12.0 v. required by the circuit and the D.C. level of the probes (except

for the mv input) was zero. This type of graph will be essential in the data reduction phase of the experiment. For instance, if the data indicates the electrometer output was + 4.0 v. it is seen on the graph that this corresponds to a differential input of - 50 mv. The data shown on this graph was taken over a period of several weeks indicating the instrument provided repeatable data.

It is seen that the upper limits of the present electrometer are ± 100 mv. There may be need to increase the range at some later time which could be done by either lowering the gain or tapping into the circuit closer to the inputs thus making a two range instrument. The instrument tested, however, has a ± 100 mv range with the upper limits on the output voltage at ± 8 volts. The graphs show voltage variations with respect to + 2.5 v. The + 2.5 v. level is the electrometer output for zero volts differential input. Since the telemetry subcarrier input range is 0 to + 5 v. and since the electrometer goes positive and negative, it is seen why the + 2.5 v. level was chosen. This level is with respect to the circuit ground and may be adjusted by the potentiometer R_{10} shown in the schematic (Figure 15). The present output of the electrometer (± 8 v.) is greater than is needed so it will be lowered by resistors before being fed into the telemetry system.

The graphs in Figures 10, 11 show the change in the electrometer when the power supplies are varied by ± 10% of their normal operating voltage (± 12.0 v.). The procedure used was to set the power supplies, find the output level for zero volts input and then apply potential differences to the input. The variations in voltage output were then plotted as a function of the differential voltage input. It is seen that the slopes of these lines do not vary considerably from the calibration curves. The main effect seems to be at the upper limits. The severest limitation

was for the positive power supply being run at - 10% of its normal voltage. It appears that small variations (< 10%) in the negative power supply can be tolerated but the positive power supply will undoubtedly have to be regulated for experimental applications.

This last effect can be seen better in Figure 12. In this case the voltage change of the + 2.5 v. level was plotted as a function of power supply variations. Here it is definitely seen that while the negative power supply variation effects are negligible, the positive power supply variations produce a change in the output voltage. The positive power supply variations are the same as if the calibration curve was raised or lowered by the amount of variation in the + 2.5 v. level. A 5% power supply variation would produce an error of approximately ± 4 mv.

Figure 13 is a graph showing the output voltage variation for D.C. level variations of both probes tied together. This graph is important since it has been shown that the probes are expected to have a floating potential. This graph shows the output variations when the probes assume floating potentials other than zero. The variation of the + 2.5 v. level due to power supply variations and floating potentials may have to be measured and used to correct the data. The variation measurement may have to be done by such calibration measurements as shorting the probes together and measuring the output relative to the "ideal case" of the + 2.5 volts. These methods will be determined for a specific project.

Figure 14 shows the frequency response of the electrometer at its upper limit. The frequency response is linear to 10 kc at which point it falls off (by 40% at 100 kc). The bandwidth may be limited further if the thermal noise (which depends on the bandwidth) is too high.

Preliminary temperature tests have been made using a "cold spray" which lowers a specific component temperature to - 20°F. This can be

sprayed on the individual components thus giving an idea of how the individual characteristics affect the circuit. These tests showed the front end FET's were most sensitive to temperature variations but fortunately in opposite directions. Large variations of the output with temperature are not expected due to this cancellation. Further testing and possible modification will be needed to meet the specifications of a specific experimental project.

For an experiment such as one on a rocket flight, certain prelaunch tests will be desirable. These would test the performance of the entire system from booms to telemetry. Shock tests and pressure tests will be performed as well as spin tests of the payload in which the boom deployment would be checked. It is also desirable to be able to supply external power to the rocket (to prevent battery run down) through an umbilical cord while the rocket is on the launcher. This cord would disconnect at launch but would provide a prelaunch period of operation to certify that the experiments are operating properly. As the needs indicate further tests will be developed.

6. Sensitivity and Accuracy Requirement

As it has been mentioned earlier in the paper, the expected electric fields in the auroral zone are on the order of 10 to 100 mv. It is expected that these fields can be measured using the collinear rocket probe arrangement and electrometer amplifier in this paper. The equation for the potential difference $\Delta\varphi$ has been found in Appendix C of the paper and is of the form

$$\Delta\varphi = (\bar{E} + \bar{v} \times \bar{B}) \cdot \bar{d} \tag{72}$$

where $\bar{d}$ is the separation of the midpoints of the probe. It is seen that

the accuracy of the electric field measurements not only depends on the actual measurement of the potential difference but also on the accuracy of determining the values of the induced potential. If one assumes 1% accuracy in these parameters (v, B, sin θ) it is not unreasonable to expect an overall accuracy in the correction calculations of 0.02 (77) mv/m $\approx$ 1.5 mv/m where 77 mv/m is the calculated induced field.

Various effects studied in the testing of the instrument and discussed in the previous section have shown that finite experimental errors exist. Some of these such as the amplifier drift due to varying D.C. probe levels and power supply variations may be corrected provided the necessary in flight calibration is done. The "ideal case" accuracy of the instrument is estimated at $\pm$ 1.0 mv. The errors due to power supply variations however are on the order (for 10% variation) of $\pm$ 4 mv. The D.C. probe level (provided it is below the breakdown limits) error can be described using the common mode rejection ratio which is the ratio of the output for a differential voltage input to the output for the same voltage applied to the two probes when they are tied together. The rejection ratio is approximately 1000 or about an error of 1% (1 mv) for an uncorrected floating potential of 1 volt.

Since the electrometer amplifier draws a current of approximately 10^{-13} amps, there will be a small error in the measured potential which is analyzed below. Following the analysis of Aggson and Heppner (1965), the leakage currents from the φ_-, φ_+ booms are I_n, I_p respectively. Using equation (61) the floating potential of the boom is

$$\varphi_o = \frac{-kT_e}{e} \text{ Ln} \left[\frac{j_e s}{\int J_+ ds + \int J_{ph}\, ds} \right] \tag{73}$$

The error in potential created by I_p is thus

$$\Delta\varphi_+ = \frac{-kT_e}{e} \operatorname{Ln} \left[\frac{-\int J_+ ds - \int J_{ph}\, ds + I_p}{\int J_+ ds + \int J_{ph}\, ds} \right] \qquad (74)$$

and by I_n

$$\Delta\varphi_- = \frac{-kT_e}{e} \operatorname{Ln} \left[\frac{-\int J_+ ds - \int J_{ph}\, ds + I_n}{\int J_+ ds + \int J_{ph}\, ds} \right] \qquad (75)$$

The error potential due to the leakage current is thus

$$\Delta(\varphi_+ - \varphi_-) = \frac{-kT_e}{e} \operatorname{Ln} \left[\frac{-\int J_+ ds - \int J_{ph}\, ds + I_p}{-\int J_+ ds - \int J_{ph}\, ds + I_n} \right] \qquad (76)$$

It is seen that for small ($\pm 10^{-11}$ amps) values of I_p, I_n (assuming exact symmetry in I_+ with a value of $\sim 10^{-8}$ amps and neglecting I_{ph}) this expression has a value of $\sim .001$ mv for $T_e = 200^{\circ}K$.

The accuracy of the data, of course, depends on all of these possible errors plus other ones of a smaller magnitude. Using the present testing information and an accurate (1%) calculation of $(\bar{v} \times \bar{B}) \cdot \bar{d}$ but with no corrections for the other effects it is felt that the measurements will be accurate to $\pm$ 5% at the 100 mv level. Lower potential differences will, of course, have higher relative errors. With the use of calibration this error is expected to be considerably reduced.

SECTION V

SUMMARY

It has been stated in theories that electric fields exist in the ionosphere and magnetosphere. These fields are believed to be closely related to the magnetic fields and are believed to be involved in the mechanisms producing auroras. It is hoped that measurements of the electric fields will lead to further clarification of these theories. These theories regarding electric fields in both the ionosphere and the magnetosphere have been briefly discussed. In the ionosphere region electric fields are thought to be produced by the high altitude ionospheric flow past the earth's magnetic field lines. In the magnetosphere circulation of a less dense charged particle plasma past the field lines creates a similar electric field.

The characteristics of charged particle motion have been discussed since this is closely related to the production of electric fields. From this study it was found that certain plasma parameters such as electron and ion thermal velocities and the Debye length will have an important influence on the method chosen to make electric field measurements in these mediums. In the ionosphere region there is expected to be no particular difficulty in designing a physically reasonable experiment while at magnetospheric altitudes this will be increasingly difficult due to the larger values of important parameters such as the mean free path and Debye length.

The theory of probe measurements of potential differences in a plasma has been studied and the effect of floating potentials, probe

movement and electron and ion currents to the probes has been discussed. Calculations of incident currents show that a high impedance electrometer amplifier is best suited for the measurements. Although the potential differences are expected to be of the order of millivolts, there will be a potential difference due to the induced field caused by the probe movement. For accurate measurements this potential must be calculated using $\overline{v}$ and $\overline{B}$ data obtained from ground tracking stations, from spherical harmonic analysis of the main field and from on-board magnetometers.

A specific electrometer amplifier using field effect input transistors has been designed. This instrument is capable of measuring millivolt potential differences without drawing a large amount of current, due to its high input impedance. It is proposed that this meter be used with an extendable boom and probe arrangement to measure the electric fields. The specific details of the instrument, boom system, and the calculations of the electric field are discussed in the last section of the paper. For the rocket project mentioned above, it is felt that electric field measurements on the order of 10 to 100 mv/m can be made with the designed instrument with an accuracy of $\pm$ 50% to $\pm$ 5%.

BIBLIOGRAPHY

Aggson, T., and J. P. Heppner, Proposal for electric field measurements on A.T.S. #1, NASA-GSFC, July, 1964.

Aggson, T., and J. P. Heppner, Proposal for electric field measurements on POGO satellites (OGO-D and OGO-F), NASA-GSFC, October, 1965.

Akasofu, S.-I., and S. Chapman, Large-scale auroral motions and polar magnetic disturbances-III, The aurora and magnetic storm of 11 February, 1958, J. Atmos. and Terres. Phys., 24, 785-796, 1962.

Alfvén, H. and C.-G. Fälthammar, Cosmical Electrodynamics, Oxford University Press, London, 1963.

Axford, W. I., and C. O. Hines, A unifying theory of high-latitude geophysical phenomena and geomagnetic storms, Canadian Journal of Physics, 39, 1433-1464, 1961.

Beard, D. B., and F. S. Johnson, Charge and magnetic field interaction with satellites, J. Geophys. Res., 65, 1-7, 1960.

Bourdeau, R. E., J. L. Donley, G. P. Serbu, and E. C. Whipple, Jr., Measurements of sheath currents and equilibrium potential on the Explorer VIII satellite, J. Astron. Sci., 8, 65-73, 1961.

Boström, R., A model for equatorial electrojets, J. Geophys. Res., 69, 4983-4999, 1964.

Cahill, L. J., Jr., A study of the outer geomagnetic field, in Space Research III, edited by W. Priester, pp. 324-330, North Holland Publishing Co., Amsterdam, 1963.

Cahill, L. J., Jr., The geomagnetic field, in Space Physics, edited by D. P. LeGalley, and A. Rosen, chap. 9, John Wiley & Sons, Inc., New York, 1964.

Cahill, L. J., Jr., The magnetosphere, Scientific American, 212, 58-68, March, 1965.

Cahill, L. J., Jr., and P. G. Amazeen, The boundary of the geomagnetic field, J. Geophys. Res., 68, 1835-1843, 1963.

Chapman, S., The electrical conductivity of the ionosphere: a review, Nuovo Cimento, suppl. 4, 1385-1412, 1956.

Chapman, S., Aurora and geomagnetic storms, in Space Physics, edited by D. P. LeGalley, and A. Rosen, chap. 7, John Wiley & Sons, Inc., New York, 1964.

Chapman, S., and J. Bartels, Geomagnetism, Vols. I and II, Clarendon Press, Oxford, 1964.

Currie, D. R., and K. S. Kreielsheimer, A double field mill for the measurement of potential gradients in the atmosphere, J. Atmos. and Terres. Phys., 19, 126-135, 1960.

Davis, L. R., O. E. Berg, and L. H. Meredith, Direct measurements of particle fluxes in and near auroras, in Space Research, edited by H. Kallman-Bijl, pp. 721-735, North Holland Publishing Co., Amsterdam, 1960.

Davis, L. R., and J. M. Williamson, Low-energy trapped protons, Space Research III, edited by W. Priester, pp. 365-375, North Holland Publishing Co., Amsterdam, 1963.

Dessler, A. J., Penetrating radiations, in Satellite Environment Handbook, edited by F. S. Johnson, pp. 49-76, University Press, 1961.

Dungey, J. W., Cosmical Electrodynamics, Cambridge University Press, 1958.

Dungey, J. W., Interplanetary magnetic field and the auroral zones, Phys. Rev. Letters, 6, 47-48, 1961.

Elsasser, W. M., The earth's interior and geomagnetism, Revs. Modern Phys., 22, 1-35, 1950.

Fahleson, U., Theory for electric field measurements in the magnetosphere with electric probes, Royal Institute of Technology Technical Report, Stockholm, Sweden, No. 66-02, 1966.

Frank, L. A., J. A. Van Allen, and E. Macagno, Charged-particle observations in the earth's outer magnetosphere, J. Geophys. Res., 68, 3543-3554, 1963.

Freden, S. C. and R. S. White, Protons in the earth's magnetic field, Phys. Rev. Letters, 3, 9-11, 1959.

Freden, S. C. and R. S. White, Particle fluxes in the inner radiation belt, J. Geophys. Res., 65, 1377-1383, 1960.

Gold, T., Motions in the magnetosphere of the earth, J. Geophys. Res., 64, 1219-1224, 1959.

Gosling, W., Field Effect Transistor Electronics, John Wiley & Sons, Inc., New York, 1958.

Hanson, W. B., Structure of the ionosphere, in Satellite Environment Handbook, edited by F. S. Johnson, pp. 27-48, University Press, 1961.

Hinteregger, H. E., K. R. Damon, and L. A. Hall, Analysis of photoelectrons from solar extreme ultraviolet, J. Geophys. Res., 64, 961-969, 1959.

Hurley, R. B., Junction Transistor Electronics, John Wiley & Sons, Inc., New York, 1958.

Imyanitov, I., and Ya. M. Shvarts, Pair of sensitive field mills on Sputnik III, Iskusstvennyye Sputniki Zemli, 17, 59-65, 1963.

Joyce, M. V., and K. K. Clarke, Transistor Circuit Analysis, Addison-Wesley, Reading, Massachusetts, 1961.

Kavadas, A., Electric Fields in the Upper Atmosphere, Research Report, Institute of Upper Atmospheric Physics, University of Saskatchewan, 1965.

Kurt, P. G., and V. I. Moroz, The potential of a metal sphere in interplanetary space, Planetary Space Science, 9, 259-268, 1962.

Langmuir, I., and H. M. Mott-Smith, The theory of collectors in gaseous discharges, Phys. Rev., 28, 727-763, 1926.

MacDonald, G. J. F., Hydromagnetic waves in space, in Space Physics, edited by D. P. LeGalley, and A. Rosen, chap. 13, John Wiley & Sons, Inc., New York, 1964.

Malmstadt, H. V., C. G. Enke, and E. C. Toren, Jr., Electronics for Scientists, W. A. Benjamin, Inc., New York, 1963.

Mapleson, W. W., and W. S. Whitlock, Apparatus for the accurate and continuous measurement of the earth's electric field, J. Atmos. and Terres. Phys., 7, 61-72, 1955.

McIlwain, C. E., Direct measurement of particles producing visible auroras, J. Geophys. Res., 65, 2727-2747, 1960.

McIlwain, C. E., Coordinates for mapping the distribution of magnetically trapped particles, J. Geophys. Res., 66, 3681-3691, 1961.

McIlwain, C. E., The radiation belts, natural and artificial, Science, 142, 355-361, 1963.

Mead, G. D., Deformation of the geomagnetic field by the solar wind, J. Geophys. Res., 69, 1181-1195, 1964.

Ness, N. F., C. S. Scearce, and J. B. Seek, Initial results of Imp-1 magnetic field experiment, J. Geophys. Res., 69, 3531-3570, 1964.

Nicolet, M., The collision frequency of electrons in the ionosphere, J. Atmos. and Terres. Phys., 3, 200-211, 1953.

Obayashi, T., and K. Maeda, Electrical states of the upper atmosphere, in Problems of Atmospheric and Space Electricity, edited by S. C. Coroniti, pp. 532-547, Elsevier, New York, 1963.

O'Brien, B. J., C. D. Laughlin, J. A. Van Allen, and L. A. Frank, Measurements of the intensity and spectrum of electrons at 1000-kilometer altitude and high latitudes, J. Geophys. Res., 67, 1209-1225, 1962.

Paltridge, G. W., Measurement of the electrostatic field in the stratosphere, J. Geophys. Res., 69, 1947-1954, 1964.

Reitz, J. R., and F. J. Milford, Plasma Physics, Foundation of Electromagnetic Theory, chap. 14, Addison-Wesley, Reading, Massachusetts, 1962.

Rosen, A., and J. L. Vogl, Cosmic rays in space, in Space Physics, edited by D. P. LeGalley, and A. Rosen, chap. 17, John Wiley & Sons, Inc., New York, 1964.

Sagalyn, R. C., Space electricity: physical problems and experimental techniques, in Problems of Atmospheric and Space Electricity, edited by S. C. Coroniti, pp. 548-565, Elsevier, New York, 1963.

Sagalyn, R. C., M. Smiddy, and J. Wisnia, Measurement and interpretation of ion density distributions in the daytime F region, J. Geophys. Res., 68, 199-211, 1963.

Schuster, A., The diurnal variation of terrestrial magnetism, Phil. Trans. London, 208, (A), 163-204, 1908.

Sevin, L. J., Jr., Field Effect Transistors, Texas Instruments, Inc., McGraw-Hill, New York, 1965.

Stewart, B., Terrestrial magnetism, Encyclopaedia Britannica, 9th ed., 1882.

Texas Instruments, Inc., Transistor Circuit Design, edited by J. A. Walston, and J. R. Miller, McGraw-Hill, New York, 1963.

Van Allen, J. A., C. E. McIlwain, and G. H. Ludwig, Radiation observations with satellite 1958 ε, J. Geophys. Res., 64, 271-286, 1959.

Whipple, E. C., Jr., Private communication, August 18, 1965.

APPENDIX A

The probe potential relative to the plasma can be calculated from the following equations in which I is the electrometer leakage current, S is the surface area of the probe, S_p is the projected surface area of the probe in a perpendicular plane (assuming a spherical probe) and v is the speed of the probe relative to the plasma (after Fahleson, 1966).

Current Balance Equation

$$I_e + I_+ + I_{ph} = I \tag{A1}$$

Electron Current

$$I_e = - SN_e e \sqrt{\frac{kT_e}{2\pi m_e}} \cdot \exp\left(\frac{e\varphi}{kT_e}\right) \tag{A2}$$

Ion Current

$$I_+ \approx S_p N_+ e \sqrt{\frac{8kT_+}{\pi m_+} + v^2} \quad (r \gg a - r) \tag{A3}$$

Photo Emission Current

$$I_{ph} = S_p J_{ph} \tag{A4}$$

Solving equation (A1) for φ, the probe potential, using equations (A2), (A3), and (A4).

$$- SN_e e \sqrt{\frac{kT_e}{2\pi m_e}} \cdot \exp\left(\frac{e\varphi}{kT_e}\right) + S_p N_+ e \sqrt{\frac{8kT_+}{\pi m_+} + v^2} + S_p J_{ph} = I \tag{A5}$$

Solving for φ we find

$$\exp\left(\frac{e\varphi}{kT_e}\right) = \left[\frac{S_p N_+ e \sqrt{\frac{8kT_+}{\pi m_+} + v^2} + S_p J_{ph} - I}{S N_e e \sqrt{\frac{kT_e}{2\pi m_e}}}\right] \tag{A6}$$

$$\varphi = \frac{-kT_e}{e} \operatorname{Ln}\left[\frac{\sqrt{\frac{kT_e}{2\pi m_e}}}{\left(\frac{N_+ S_p}{N_e S}\right)\sqrt{\frac{8kT_+}{\pi m_+} + v^2} + \left(\frac{S_p}{S}\right)\frac{J_{ph}}{N_e e} - \frac{I}{S N_e e}}\right] \tag{A7}$$

The floating potential is found by letting $I = 0$ in equation (A7).

APPENDIX B

One of the most difficult parts of an electric field measurement experiment is expected to be the analysis of the data. In-flight calibration techniques will be used to determine the amplifier drift due to the changing potential levels of the probes as well as changes due to temperature variations and similar effects.

The source of the largest error is the induced $\bar{v} \times \bar{B}$ field which has been shown to produce potential differences of a similar magnitude to those created by the electric field being measured. The $\bar{v} \times \bar{B}$ field cannot be neglected and it must be computed from data gained from rocket-borne magnetometers and ground tracking stations which will provide data on the magnetic field, the rocket velocity and its position relative to the magnetic field. Once the induced potential has been determined, appropriate corrections to the data can be made.

Much of the data analysis will be accomplished by programs similar to the one written by the author and shown below. This program was written in FORTRAN for the CDC 3600 computer. The program consists of several DO loops which substitute various parameters in the $(\bar{v} \times \bar{B}) \cdot \bar{d}$ equation to determine the potential due to the induced field.

```
    PROGRAM FIVE
C   (v x B)·d FOR SOUNDING ROCKET
    PRINT 400
400 FORMAT(11H1MAG. FIELD,5X,5HTHETA,5X,8HVELOCITY,5X,7H POTL    ,5X,
   15HPROBE,/11H    GAUSS   ,15X,8H KM./SEC,5X,7H MV     ,5X,5H   CM.,//)
    DO 100 J = 100, 250, 15
    DO 200 K = 1, 12
    DO 300 I = 1, 9, 2
    DO 600 L = 7, 15, 2
    X = (K - 1)/ 10.
    B = (I - 1)/ 10.
    H = J*B*L*SINF(X)
```

```
      PRINT 500, (B,X,J,H,L)
  500 FORMAT(1X,F10.3,2X,F8.3,3X,I8,8X,F7.2,7X,I5)
  600 CONTINUE
  300 CONTINUE
  200 CONTINUE
  100 CONTINUE
      END
```

APPENDIX C

The potential difference $\Delta\varphi$ which will be measured for the rocket probe configuration shown in Figure 6 can be calculated using the current balance equation.

Current Balance Equation

$$\int J_e ds + \int J_+ ds + \int J_{ph} ds = 0 \qquad (C1)$$

Electron Current Density

$$J_e = - j_e \exp \left[\frac{e(\varphi + [\bar{E} + \bar{v} \times \bar{B}] \cdot \bar{r})}{kT_e} \right] \qquad (C2)$$

Solving for the potential, φ_+, of the right hand boom in Figure 6 where a is the probe radius (after Aggson and Heppner, 1965).

$$2\pi a j_e \int_{\bar{d}_1}^{\bar{d}_2} \exp \left[\frac{e(\varphi_+ + [\bar{E} + \bar{v} \times \bar{B}] \cdot \bar{r})}{kT_e} \right] dr = \int J_+ ds + \int J_{ph} ds \qquad (C3)$$

$$2\pi a j_e \left[\frac{kT_e}{e(\bar{E}+\bar{v}\times\bar{B})} \right] \left[\exp\left(\frac{e(\bar{E}+\bar{v}\times\bar{B})\cdot\bar{d}_2}{kT_e} \right) - \exp\left(\frac{e(\bar{E}+\bar{v}\times\bar{B})\cdot\bar{d}_1}{kT_e} \right) \right] \exp\left(\frac{e\varphi_+}{kT_e} \right) =$$

$$\int J_+ ds + \int J_{ph} ds \qquad (C4)$$

Solving for φ_+

$$\varphi_+ = \frac{-kT_e}{e} \operatorname{Ln}\left[\left(\frac{2\pi a j_e \left|\frac{kT_e}{e(\bar{E}+\bar{v}x\bar{B})}\right|}{\int J_+ ds + \int J_{ph} ds}\right) \cdot \left(\exp\left[\frac{e(\bar{E}+\bar{v}x\bar{B})\cdot\bar{d}_2}{kT_e}\right] - \exp\left[\frac{e(\bar{E}+\bar{v}x\bar{B})\cdot\bar{d}_1}{kT_e}\right]\right)\right] \quad (C5)$$

Solving similarly for φ_-, the potential of the other probe we find

$$\varphi_- = \frac{-kT_e}{e} \operatorname{Ln}\left[\left(\frac{2\pi a j_e \left|\frac{kT_e}{e(\bar{E}+\bar{v}x\bar{B})}\right|}{\int J_+ ds + \int J_{ph} ds}\right) \cdot \left(\exp\left[\frac{-e(\bar{E}+\bar{v}x\bar{B})\cdot\bar{d}_1}{kT_e}\right] - \exp\left[\frac{-e(\bar{E}+\bar{v}x\bar{B})\cdot\bar{d}_2}{kT_e}\right]\right)\right] \quad (C6)$$

To find $\Delta\varphi$, the potential difference between the probes, subtract (C5) from (C6).

$$\Delta\varphi = \varphi_- - \varphi_+ = \frac{-kT_e}{e} \operatorname{Ln}\left[\frac{\exp\left(\frac{-e(\bar{E}+\bar{v}x\bar{B})\cdot\bar{d}_1}{kT_e}\right) - \exp\left(\frac{-e(\bar{E}+\bar{v}x\bar{B})\cdot\bar{d}_2}{kT_e}\right)}{\exp\left(\frac{e(\bar{E}+\bar{v}x\bar{B})\cdot\bar{d}_2}{kT_e}\right) - \exp\left(\frac{e(\bar{E}+\bar{v}x\bar{B})\cdot\bar{d}_1}{kT_e}\right)}\right] \quad (C7)$$

which can be reduced to

$$\Delta\varphi = (\bar{E} + \bar{v} \times \bar{B}) \cdot (\bar{d}_1 + \bar{d}_2) \quad (C8)$$

where $\bar{d}_1 + \bar{d}_2$ is d, the separation between the centers of the two collinear probes as can be seen below.

$$d = \left(\frac{\bar{d}_1 + \bar{d}_2}{2}\right) - \left(\frac{-\bar{d}_1 - \bar{d}_2}{2}\right) = \bar{d}_1 + \bar{d}_2 \quad (C9)$$

TABLE 1

PLASMA PARAMETERS

Altitude km	Conditions	Ion Density m^{-3}	Ion Temperature ^{o}K	Electron Temperature ^{o}K	Magnetic Field gauss	Electron Debye Length m	Ion Gyro Radius m	Electron Gyro Radius m	Mean Free Path m
80	night	3×10^{3}	200	200	0.5	6×10^{-2}	2	10^{-2}	10^{-2}
80	day	10^{9}	200	200	0.5	3×10^{-2}	2	10^{-2}	10^{-2}
120	night	10^{9}	300	300	0.5	4×10^{-2}	2	10^{-2}	1
120	aurora	10^{12}	400	500 ?	0.5	2×10^{-3}	3	10^{-2}	1
120	day	10^{11}	400	400	0.5	4×10^{-3}	3	10^{-2}	1
300	night	3×10^{11}	700	10^{3}	0.45	4×10^{-3}	3	2×10^{-2}	10^{3}
300	day	10^{12}	1800	2×10^{3}	0.45	3×10^{-3}	5	3×10^{-2}	10^{3}
3000	day	5×10^{9}	3×10^{3}	3×10^{3}	0.16	5×10^{-2}	9	10^{-1}	10^{5}
30000	day	3×10^{8}	3×10^{4}?	3×10^{4}?	7×10^{-3}	0.7	300	8	10^{6}
50000	day	10^{6}	3×10^{5}?	3×10^{5}?	7×10^{-4}	40	10^{4}	200	10^{8}

(Fahleson, 1966)

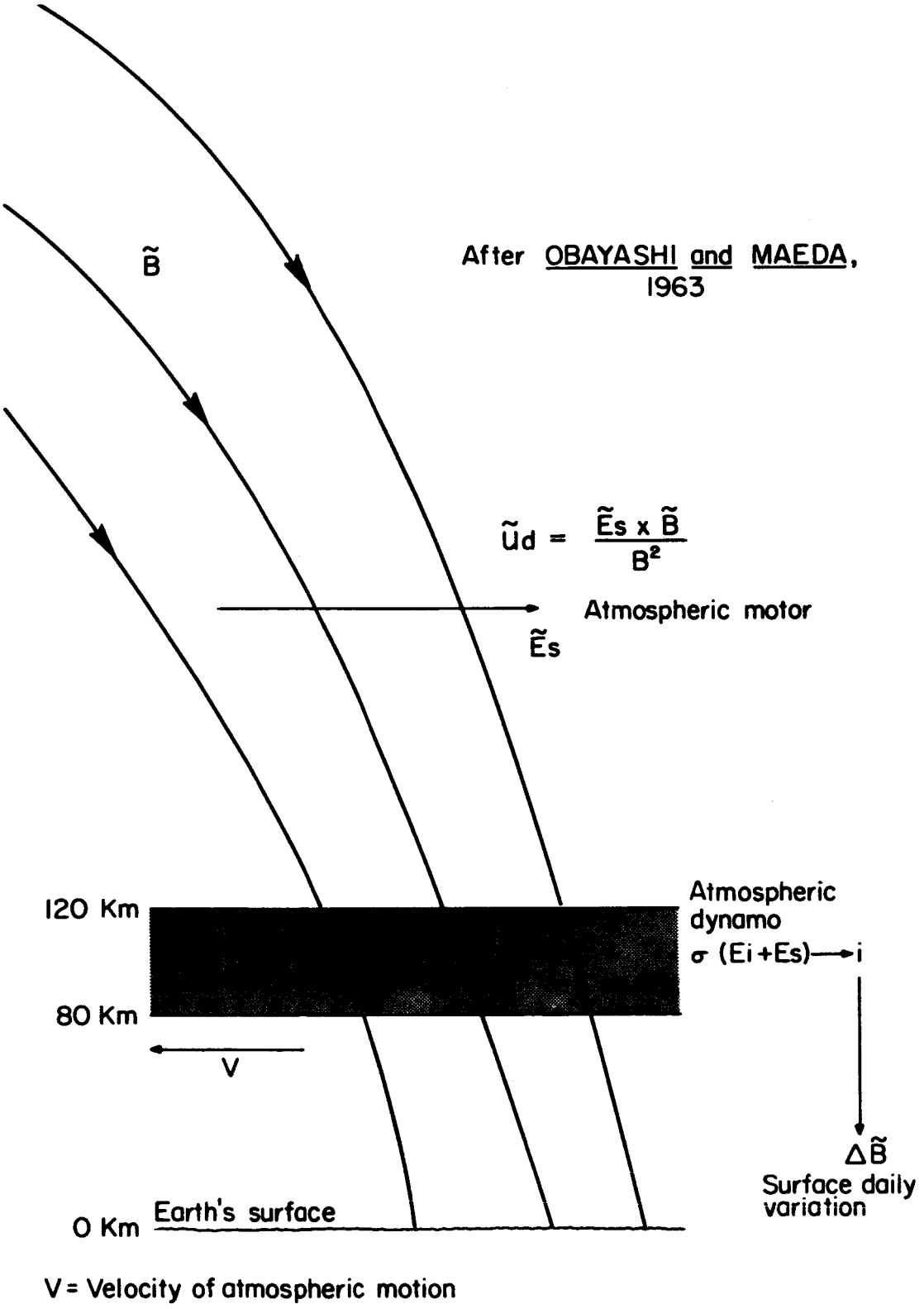

ATMOSPHERIC MOTOR–DYNAMO SYSTEM

Figure 1

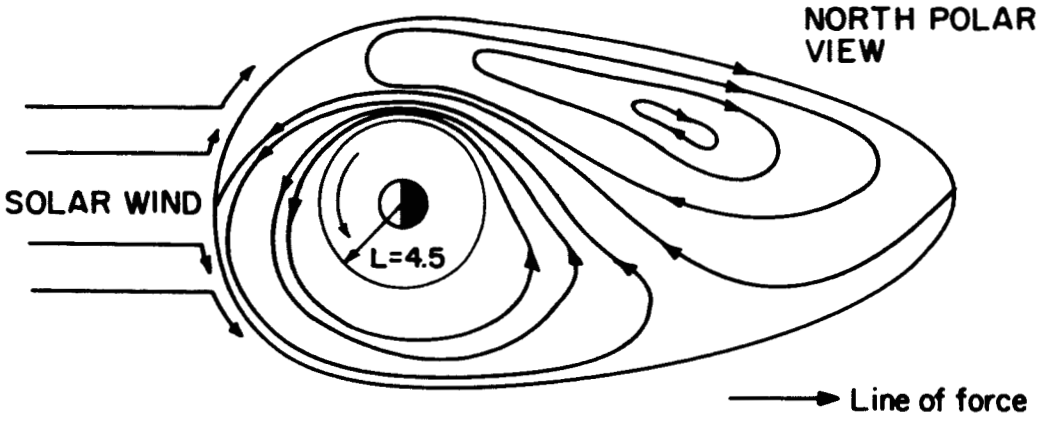

CLOSED MODEL

(a)

After AXFORD and HINES, 1961

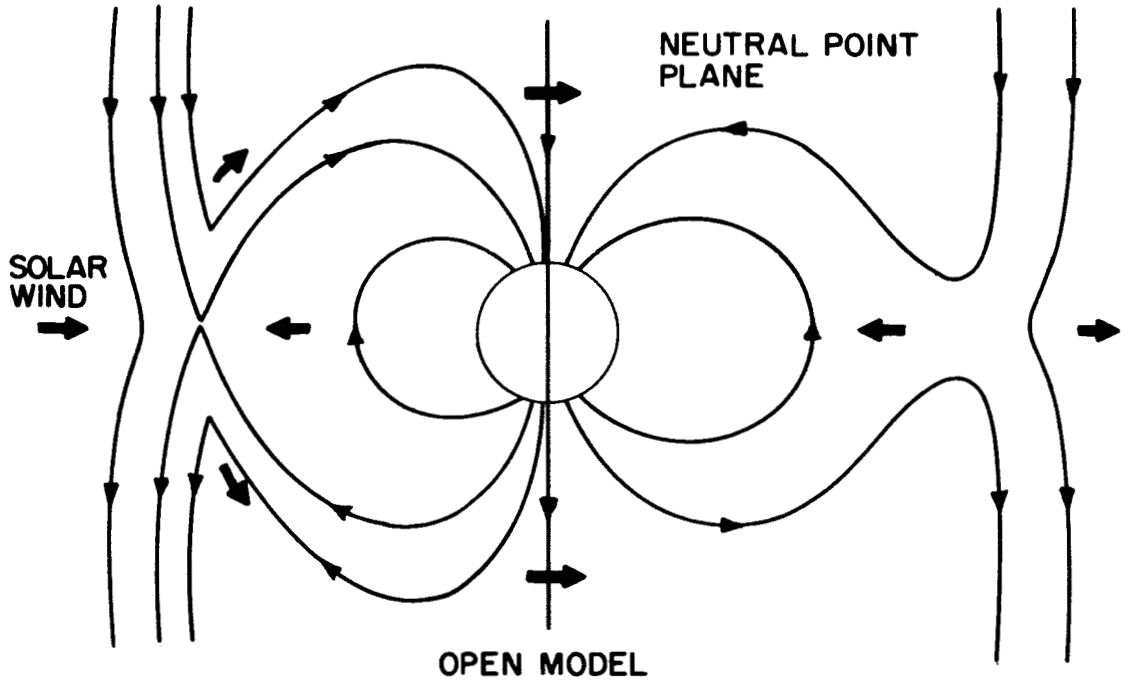

OPEN MODEL

After DUNGEY, 1961

(b)

Flow direction

Line of force

MAGNETOSPHERE PLASMA CONVECTION THEORIES

Figure 2

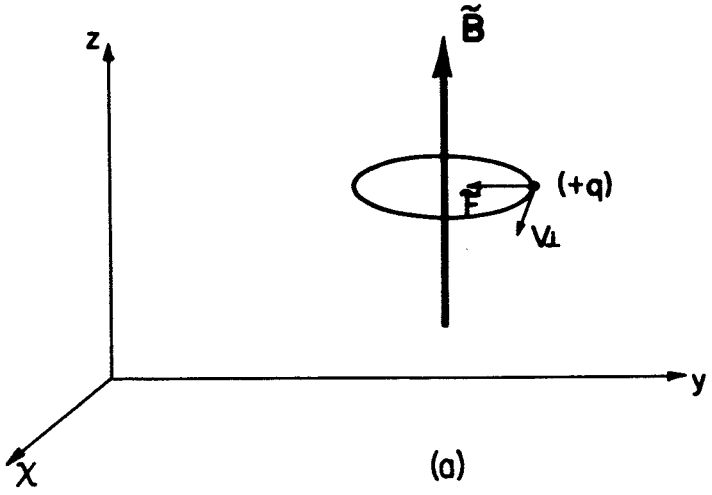

(a)

$\tilde{B}$ uniform
$\tilde{E}$ =0
Velocity with respect to B
$V_\perp \neq 0$
$V_{||} = 0$
Circle radius $R = \frac{mV_\perp}{qb}$
Force $\tilde{F} = q\,\tilde{V}_\perp \times \tilde{B}$

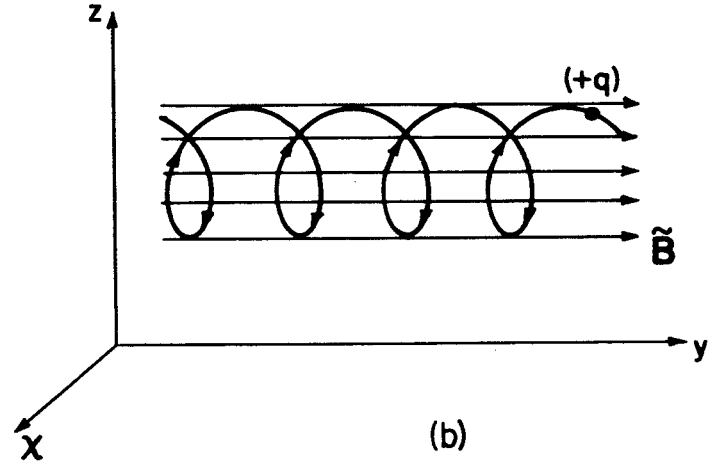

(b)

$\tilde{B}$ uniform
$\tilde{E}$ =0
$V_\perp \neq 0$
$V_{||} \neq 0$
Helix radius $R = \frac{mV_\perp}{qB}$

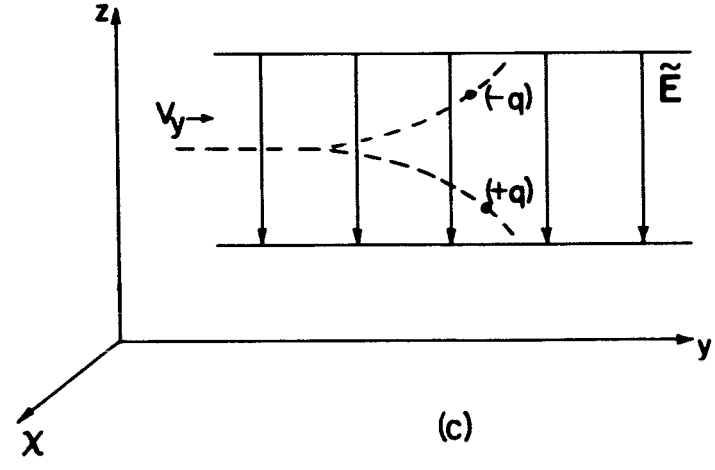

(c)

$\tilde{B}$ =0
$\tilde{E}$ uniform
V_x =0
$V_y \neq 0$
V_z =0

PARTICLE MOTION IN $\tilde{E}$ AND $\tilde{B}$ FIELDS

Figure 3

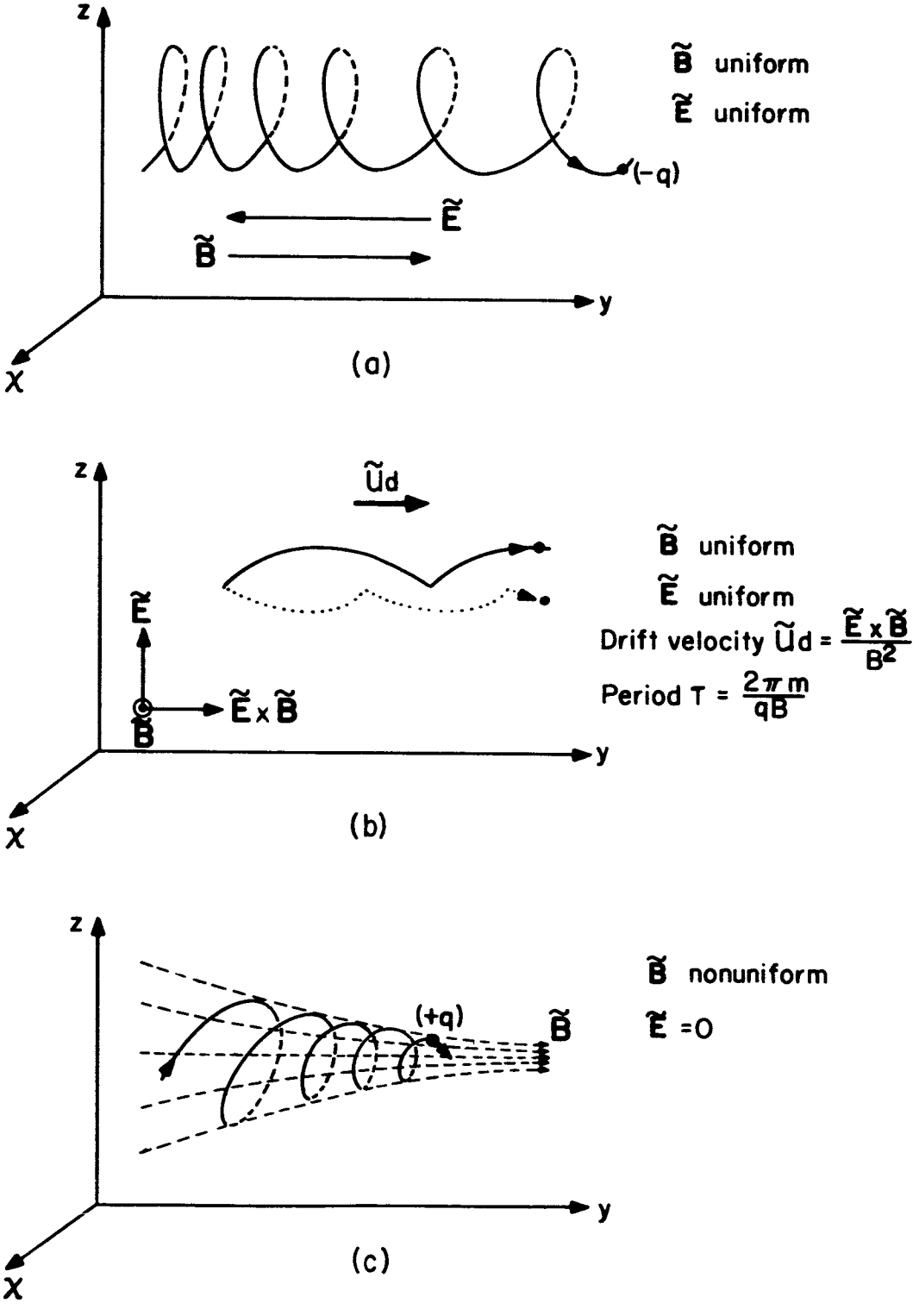

PARTICLE MOTION IN $\tilde{E}$ AND $\tilde{B}$ FIELDS

Figure 4

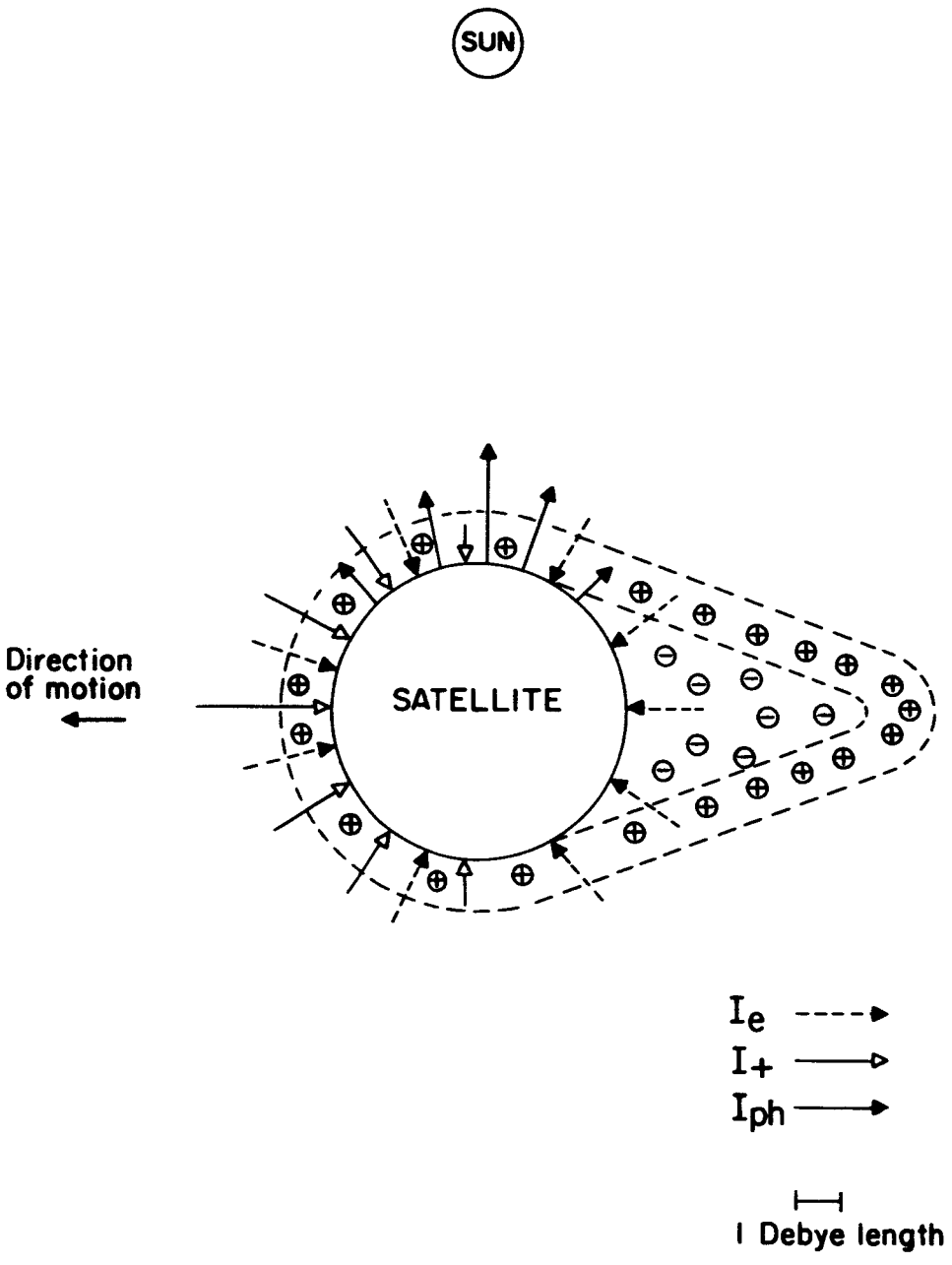

POSTULATED SHEATH MODEL OF EXPLORER VIII
AFTER BOURDEAU, et al, 1961

Figure 5

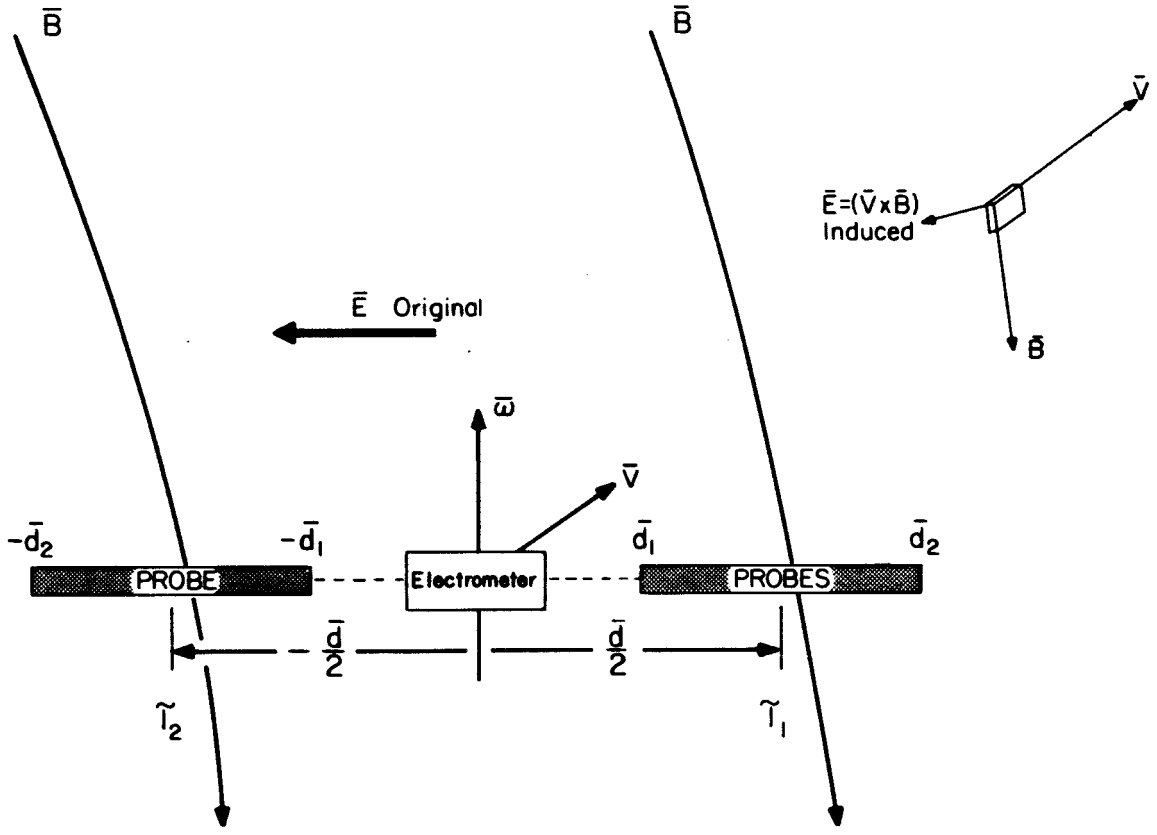

$\Delta\phi = \Delta\phi_o + \Delta\phi_1$ Potential difference between $\tilde{l}_1$ and $\tilde{l}_2$

$\Delta\phi_o = E\,d\,\cos(\bar{d},\bar{E})$

$\Delta\phi_1 = vBd\,\sin(\bar{v},\bar{B})\,\cos(\bar{v}\times\bar{B},\bar{d})$

THE $\tilde{V}\times\tilde{B}$ EFFECT FOR COLLINEAR CYLINDRICAL PROBES

Figure 6

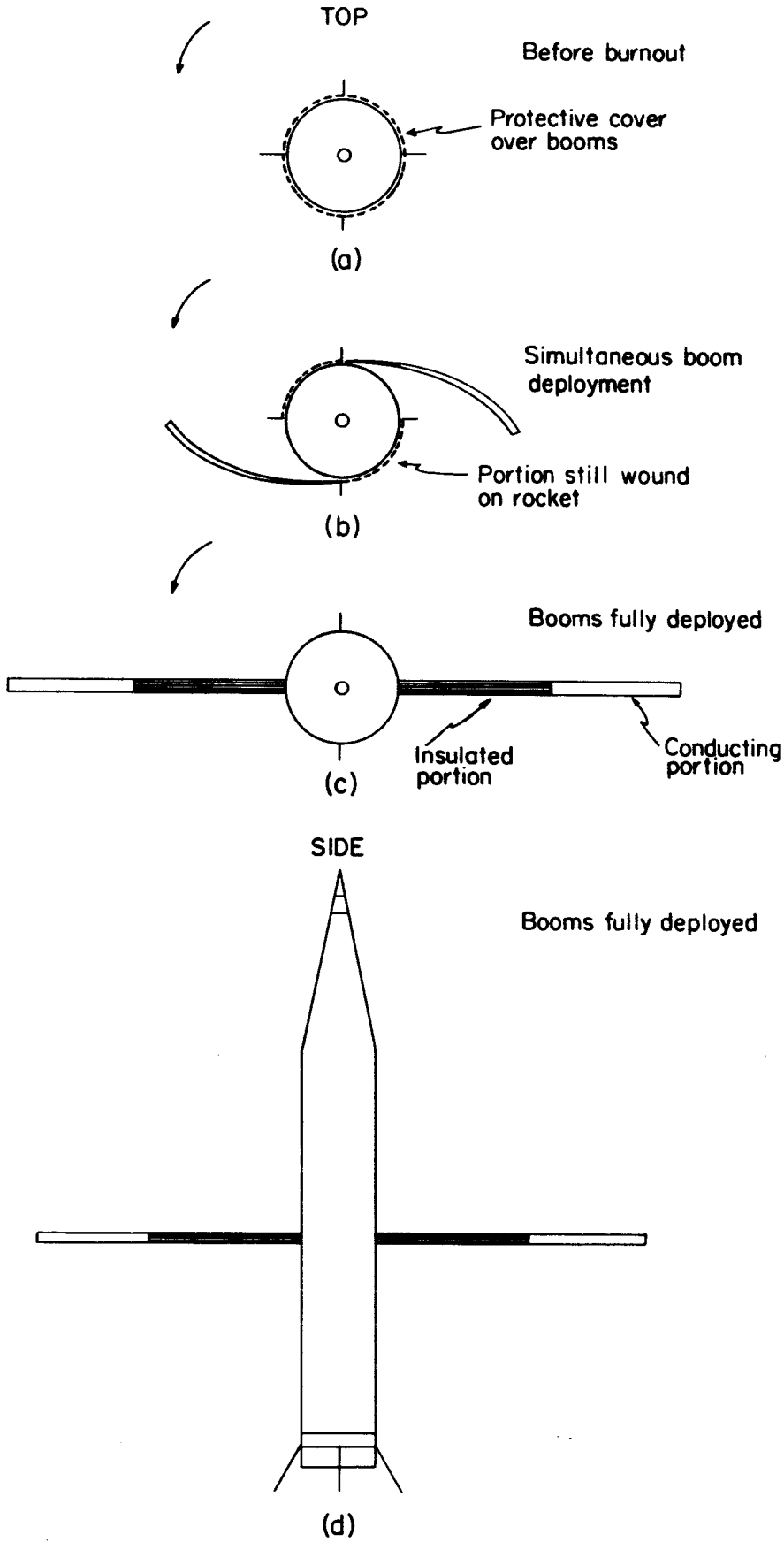
TOP
Before burnout
Protective cover over booms
(a)
Simultaneous boom deployment
Portion still wound on rocket
(b)
Booms fully deployed
Insulated portion
Conducting portion
(c)
SIDE
Booms fully deployed
(d)

Figure 7

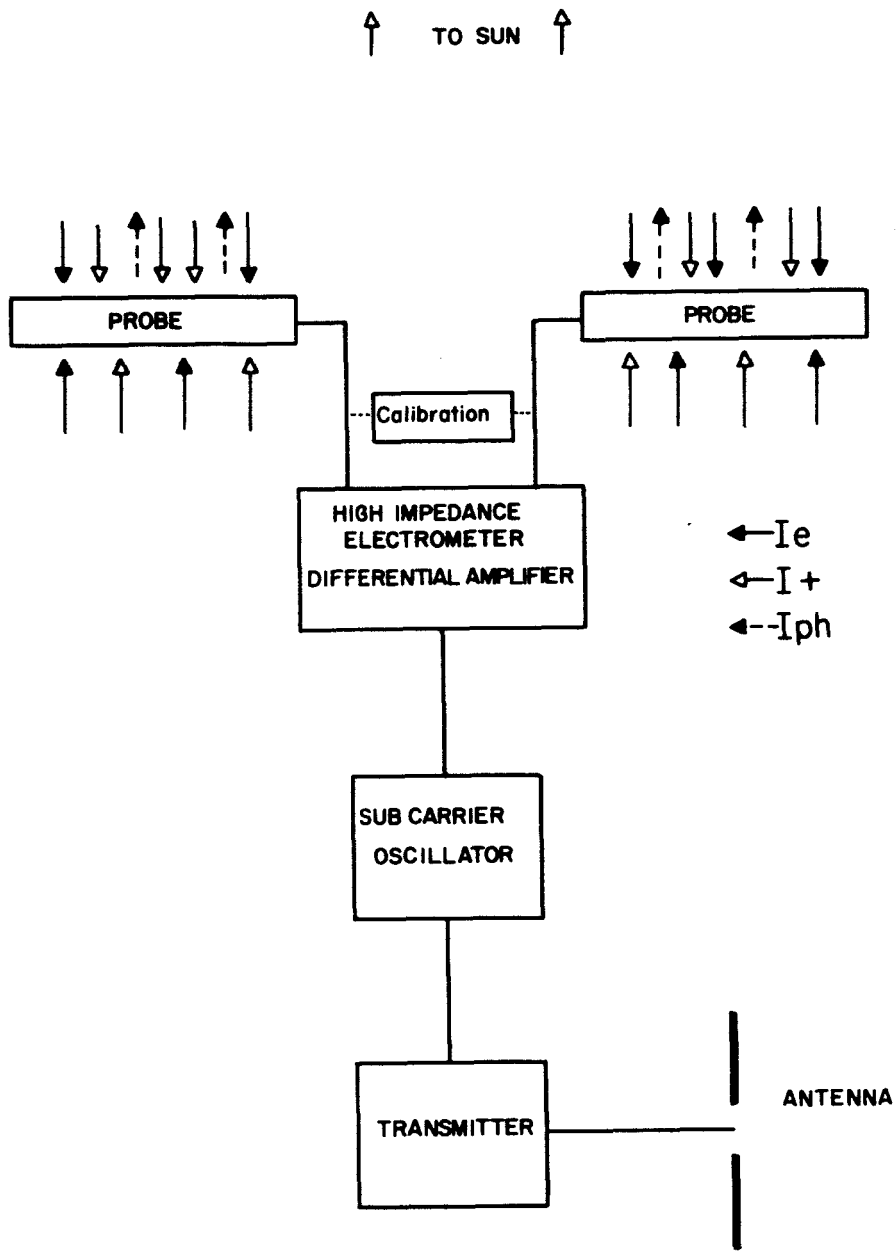

ELECTRIC FIELD MEASURING TECHNIQUE

Figure 8

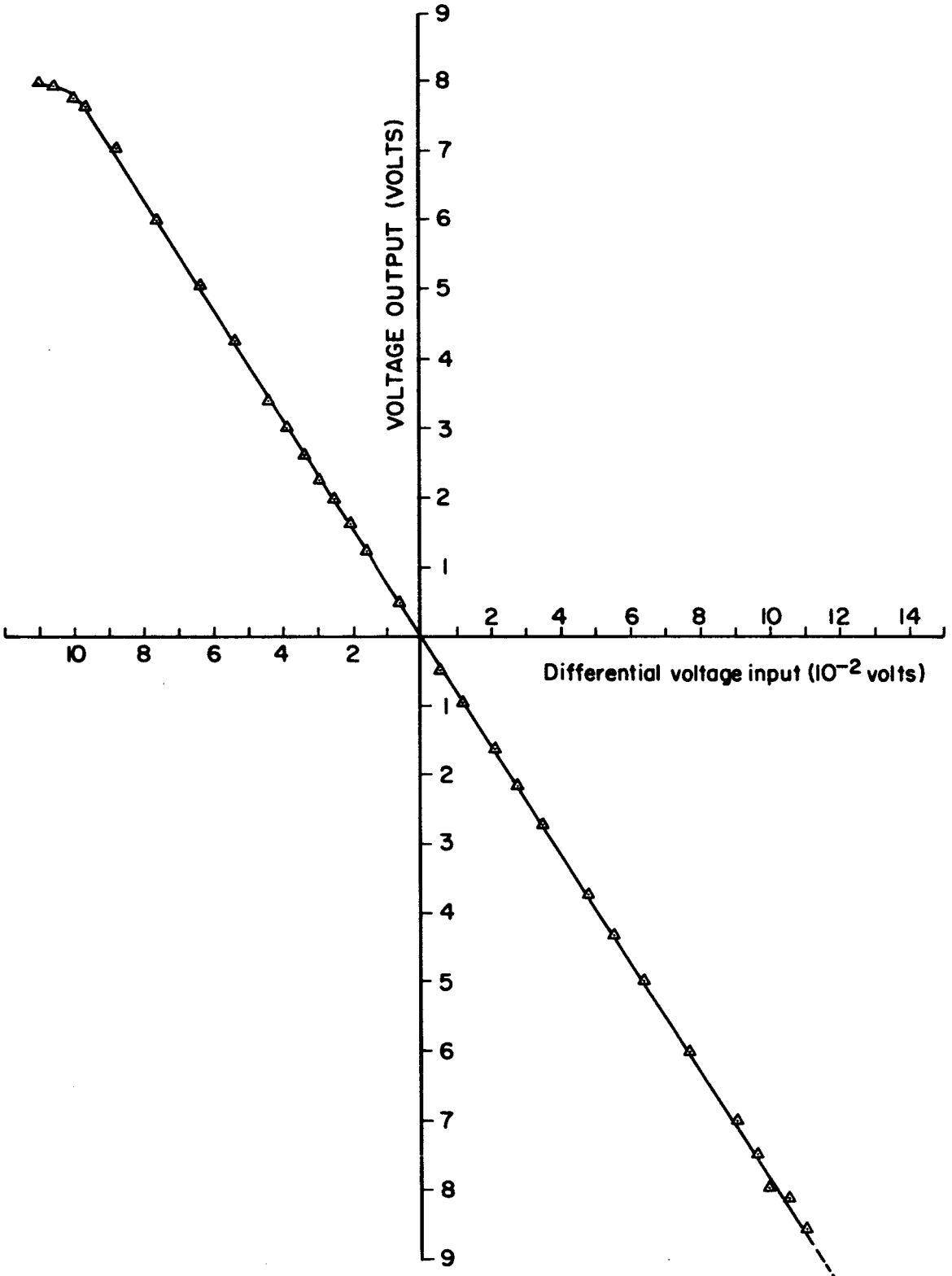

CALIBRATION CURVE–ELECTROMETER AMPLIFIER

Differential volts IN vs volts OUT

Figure 9

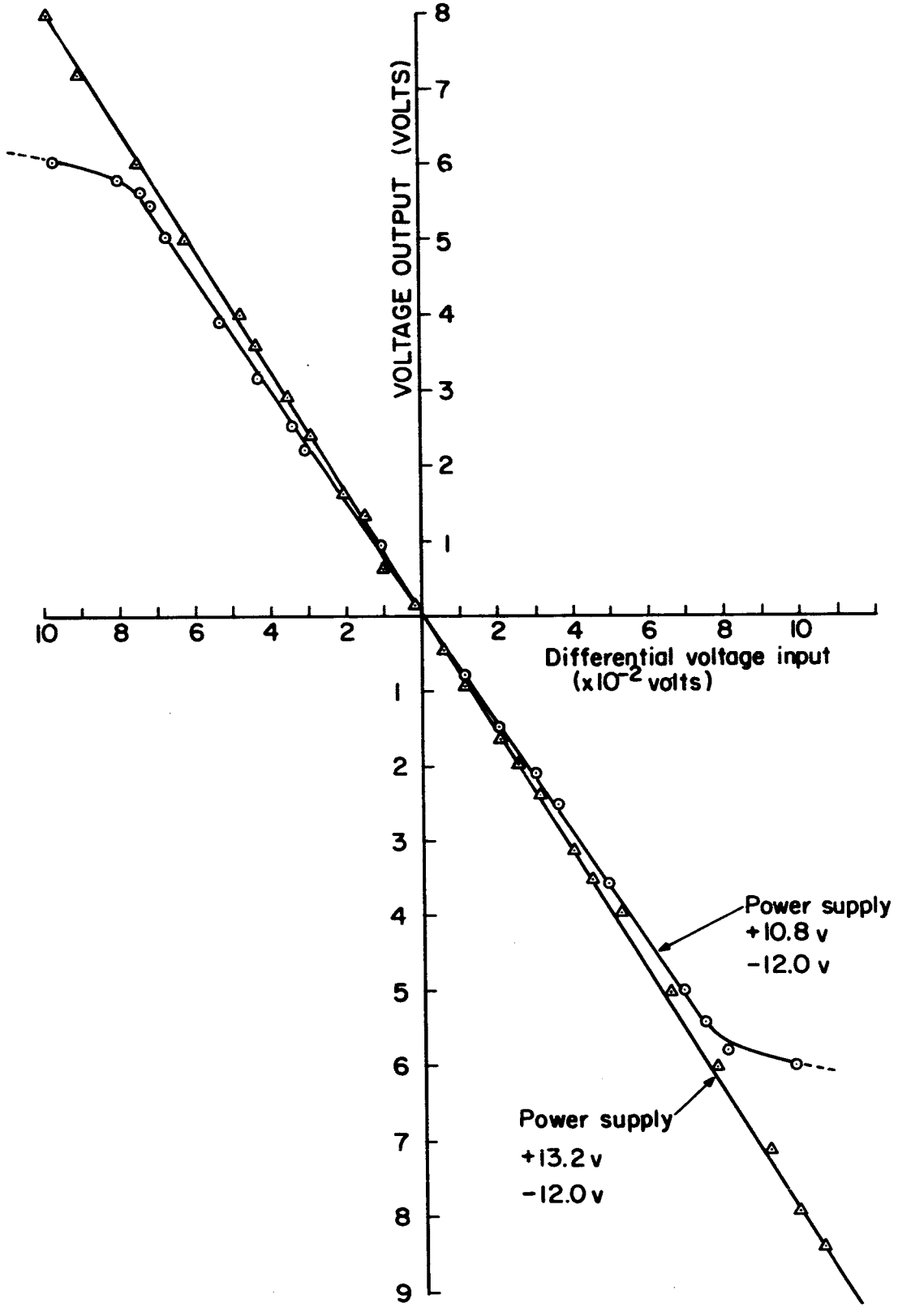

POWER SUPPLY VARIATION EFFECTS (±10%)
Differential volts IN vs volts OUT

Figure 10

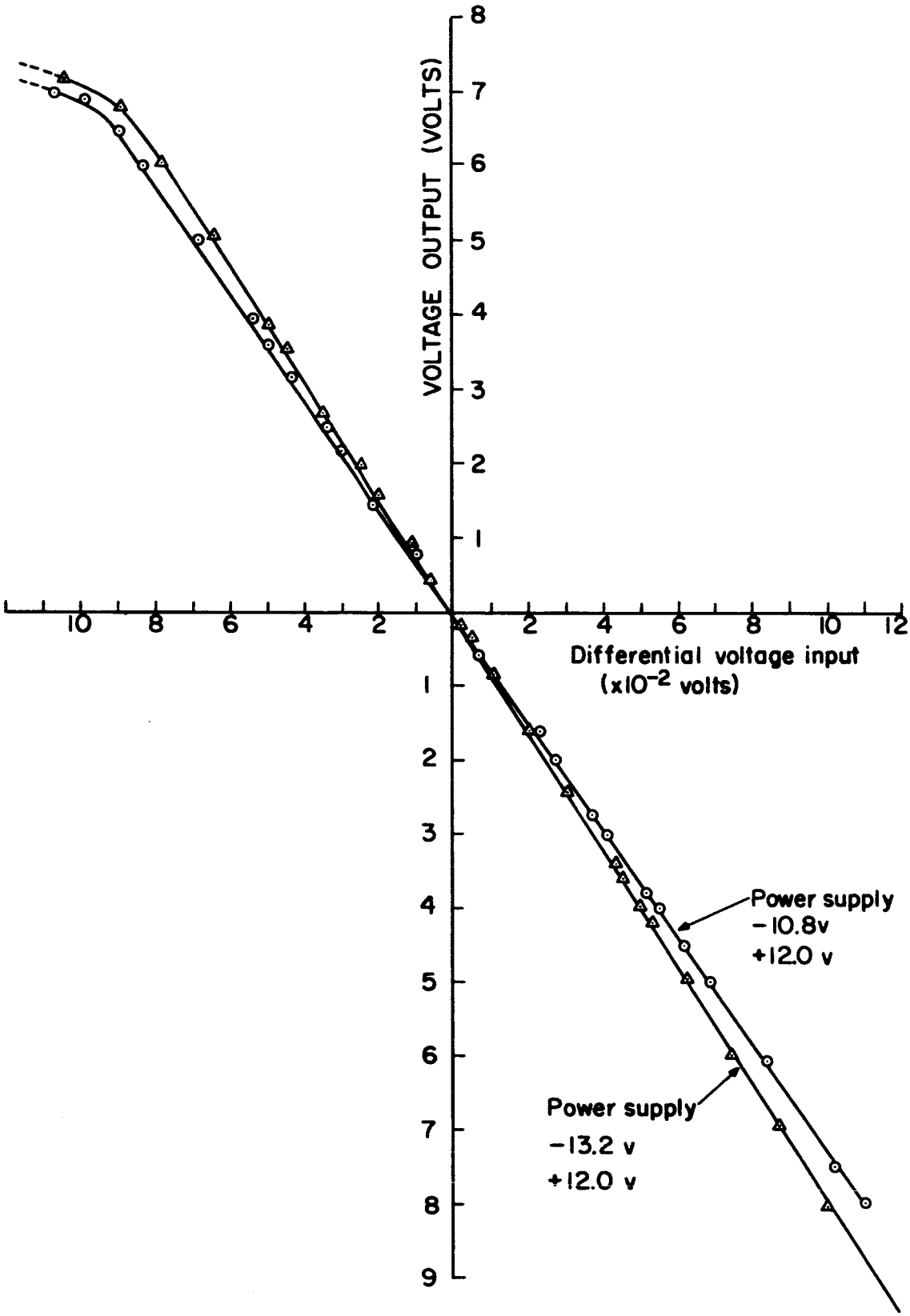

POWER SUPPLY VARIATION EFFECTS (±10%)
Differential volts IN vs volts OUT

Figure 11

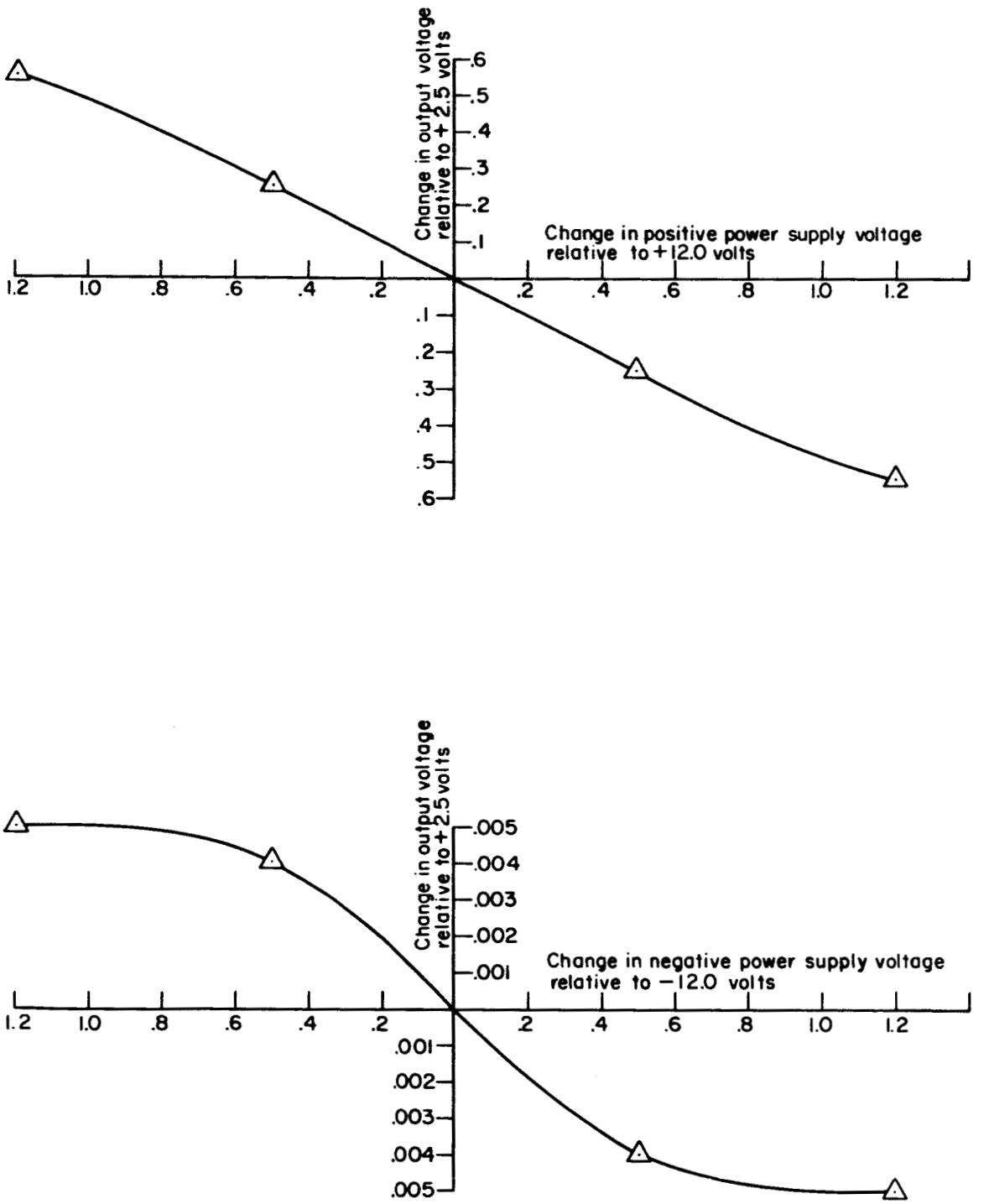

CHANGES OF OUTPUT VOLTAGE FOR ZERO INPUT AND POWER SUPPLY VARIATIONS

Figure 12

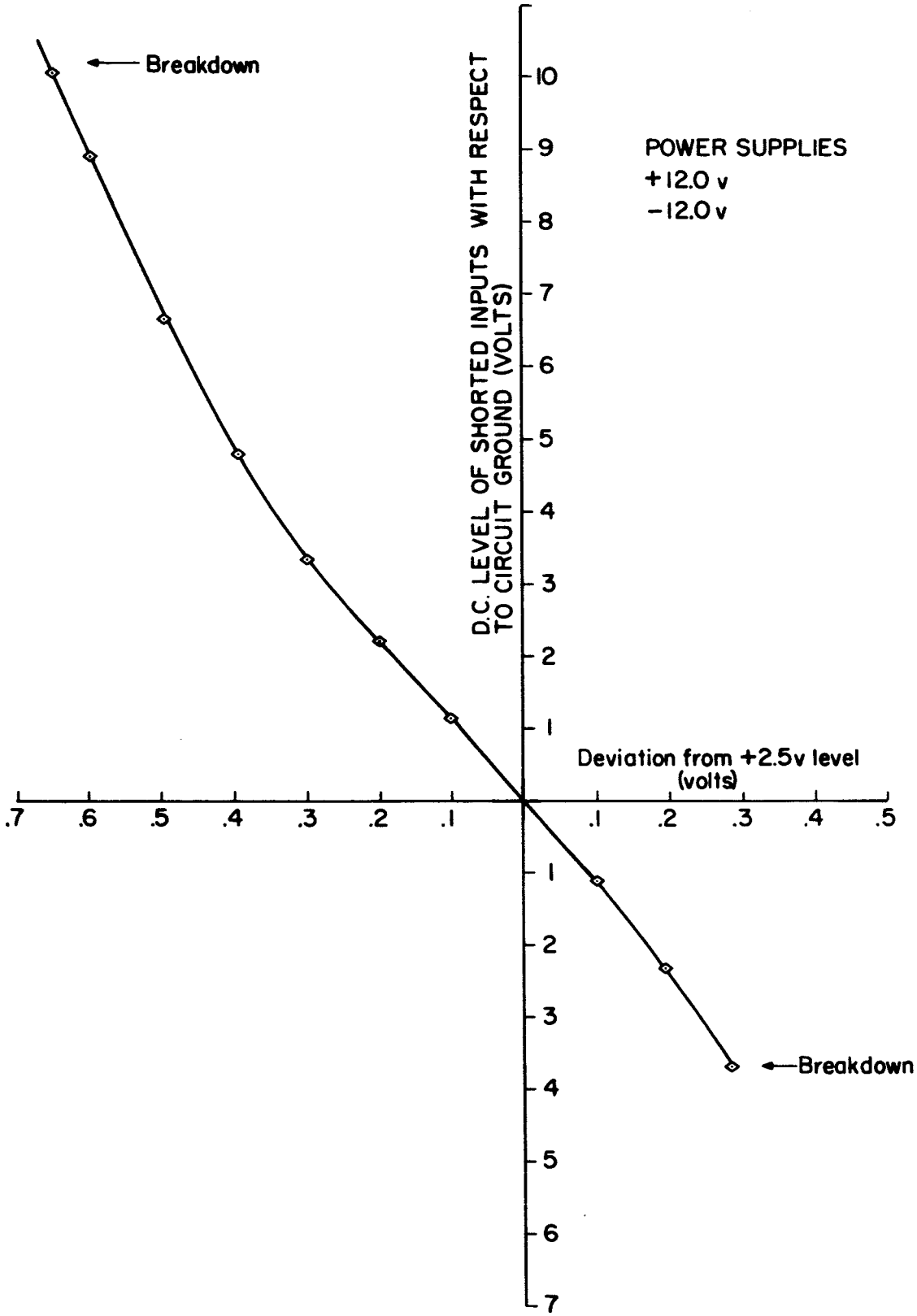

DEVIATIONS OF OUTPUT DUE TO VARYING D.C. PROBE LEVELS
D.C. level vs deviation

Figure 13

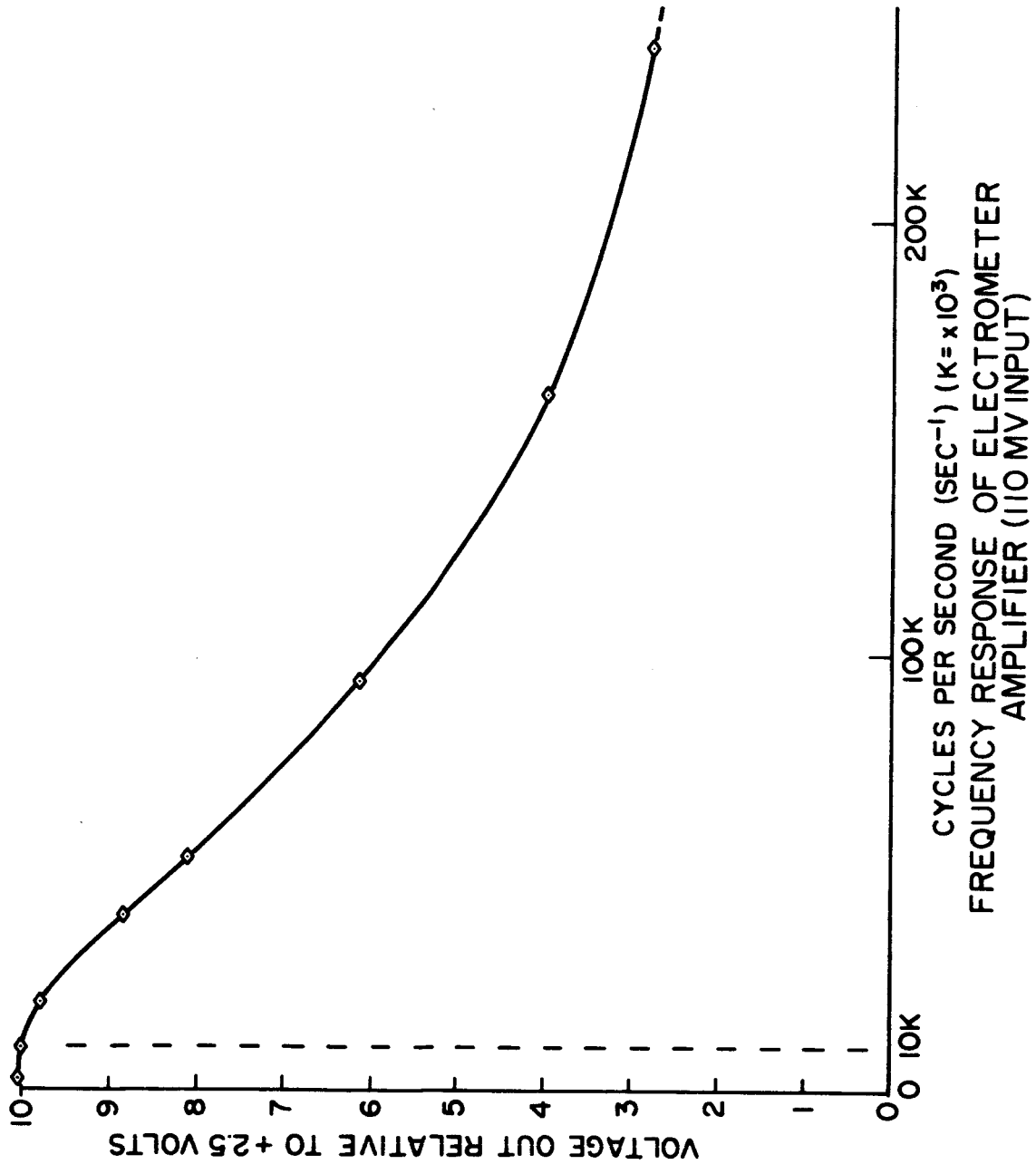
VOLTAGE OUT RELATIVE TO +2.5 VOLTS
10
9
8
7
6
5
4
3
2
1
0
0 10K
100K
200K
CYCLES PER SECOND (SEC⁻¹) (K = x 10³)
FREQUENCY RESPONSE OF ELECTROMETER AMPLIFIER (110 MV INPUT)

Figure 14

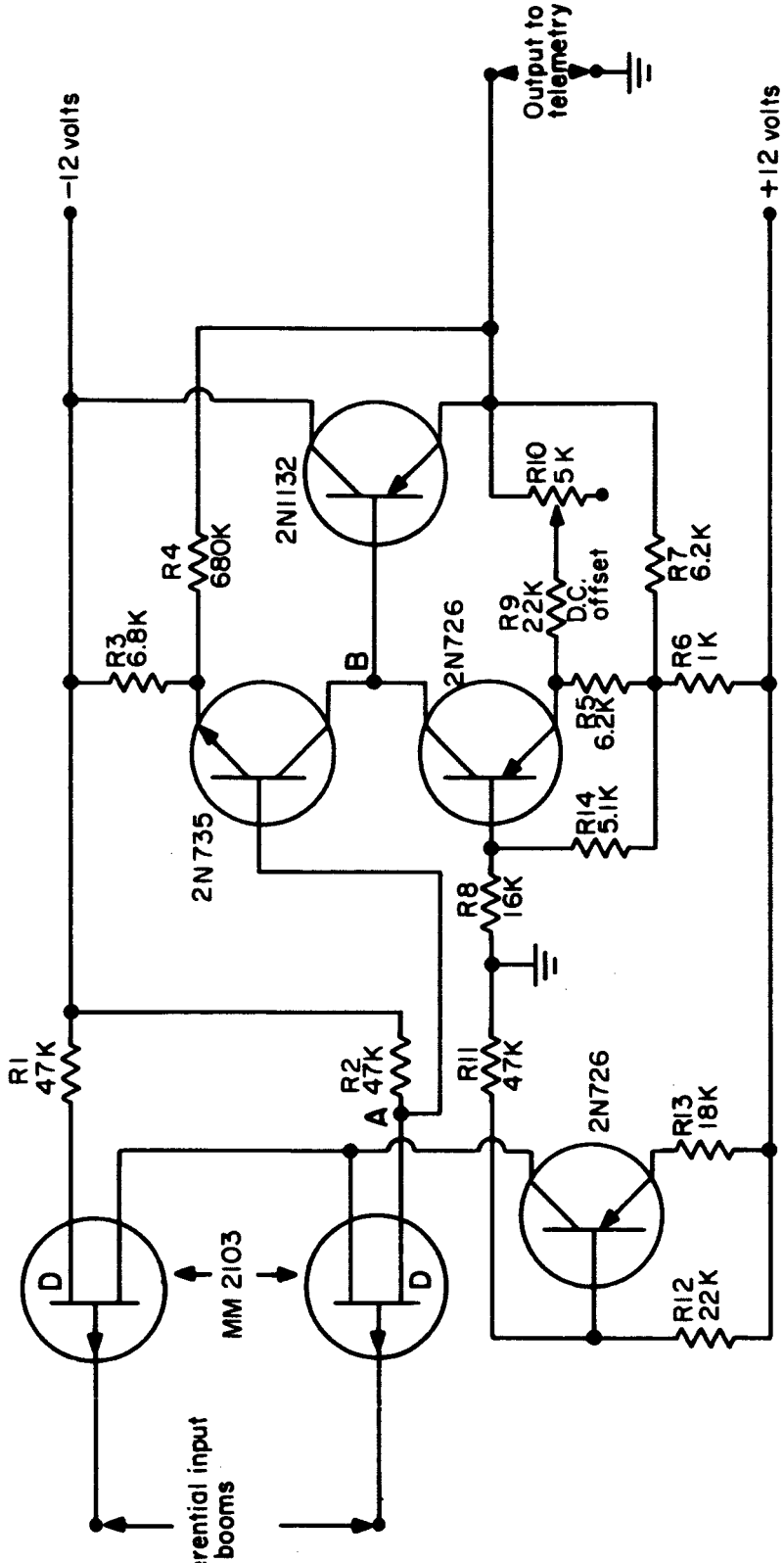

F.E.T. HIGH IMPEDANCE DIFFERENTIAL ELECTROMETER AMPLIFIER

Figure 15